UNIVERSITY OF LEEDS

This is a repository copy of *A transfer function method to predict building vibration and its application to railway defects*.

White Rose Research Online URL for this paper:
http://eprints.whiterose.ac.uk/153360/

Version: Accepted Version

Article:
López-Mendoza, D, Connolly, DP, Romero, A et al. (2 more authors) (2020) A transfer function method to predict building vibration and its application to railway defects. Construction and Building Materials, 232. 117217. ISSN 0950-0618

https://doi.org/10.1016/j.conbuildmat.2019.117217

© 2019 Elsevier Ltd. All rights reserved. This manuscript version is made available under the CC-BY-NC-ND 4.0 license http://creativecommons.org/licenses/by-nc-nd/4.0/.

Reuse
This article is distributed under the terms of the Creative Commons Attribution-NonCommercial-NoDerivs (CC BY-NC-ND) licence. This licence only allows you to download this work and share it with others as long as you credit the authors, but you can't change the article in any way or use it commercially. More information and the full terms of the licence here: https://creativecommons.org/licenses/

Takedown
If you consider content in White Rose Research Online to be in breach of UK law, please notify us by emailing eprints@whiterose.ac.uk including the URL of the record and the reason for the withdrawal request.

White Rose university consortium
Universities of Leeds, Sheffield & York

eprints@whiterose.ac.uk
https://eprints.whiterose.ac.uk/

A transfer function method to predict building vibration and its application to railway defects

D. López-Mendoza[a], D.P. Connolly[b], A. Romero[a], G. Kouroussis[c], P. Galvín[*,a]

[a] *Escuela Técnica Superior de Ingeniería, Universidad de Sevilla, Camino de los Descubrimientos s/n, 41092 Sevilla, Spain*
[b] *Institute for High Speed Rail and Systems Integration, Civil Engineering, University of Leeds, UK*
[c] *Faculty of Engineering, Department of Theoretical Mechanics, Dynamics and Vibrations, Université de Mons, Belgium*

Abstract

This work presents a simplified method to evaluate building shaking due to arbitrary base excitations, and an example application to railway problems. The model requires minimal computational effort and can be applied to a wide range of footing shapes, thus making it attractive for scoping-type analysis. It uses the soil excitation spectrum at the building footing location as it's input, and computes the building response at any arbitrary location within it's 3D structure. To show an application of the model versatility, it is used to compute building response due to a variety of singular railway defects (e.g. switches/crossings). It is however suitable for more general applications including general railway problems. The approach is novel because current railway scoping models do not use soil-structure transfer functions combined with free-field response to estimate building vibration by railway defects. First the soil-structure interaction approch is outlined for both rigid and flexible footings. Then it is validated by comparing results against a comprehensive fully-coupled 3D FEM-BEM model. Finally, it is used to analyse the effect of a variety of variables (soil properties, defect type, defect size and train speed) on 3 different buiding types. Overall the new approach allows for the computation of building vibrations with high accuracy, using minimal computational effort.

Key words: Ground-borne vibrations, Railway traffic, High speed rail, Building vibrations, Structural vibration, Environmental Impact Assessment (EIA), Railway singular defects

1. Introduction

The response of structures to ground-borne waves induced by blasting, earthquake, road and railway traffic, are examples where soil-structure interaction (SSI) is an important issue and its influence cannot be neglected [1, 2].

The importance to consider SSI in the building response due to blast-induced ground motion, was analysed by Wu and Hao [3, 4]. They proposed a numerical model to predict surface ground motion due

[*]Corresponding author. Tel.: +34 954487293
Email address: pedrogalvin@us.es (P. Galvín)

to underground blasting. These free-field response was used as input excitation to obtain the building response using a simple approach, where the source (blasting)-receiver (building) interaction was neglected. Bayraktar et al. [5] developed a detailed nonlinear dynamic analysis of concrete and masonry structures using an hybrid approach. The ground excitations due to blasting was measured and combined with a numerical building model updated with experimental dynamic characteristics. Dogan et al. [6] presented a combined experimental/numerical procedure to obtain the building response due to blasting. Ground motion was measured while building vibration was computed using a 3D model where the SSI was ignored. A comparison between underground and surface blasts was developed and it was found smaller vibrations for the underground case.

On the other hand, the pronounced effect of SSI on the structure response for softer layered soils was analysed by Savin et al. [7] in seismic problems, using a detailed 3D model. Gatti et al. [8] presented a complete approach from the source (earthquake) to the structure. The wave-motion was used as input motion for a SSI numerical BEM-FEM model for a reactor building. Alternatively, simplified procedures [9–11] were proposed to model SSI in seismic analysis.

Numerical models to compute building vibrations by road traffic include Pyl et. al [12, 13] who presented a complete coupled boundary element (BEM)- finite element (FEM) methodology to analyse the road-soil-structure system. Alternatively, François et al. [14] studied dynamic building behaviour considering the relative stiffness between the building and the soil to simplify modelling soil-structure interaction (SSI).

Regarding the rail sector, the growth of urban railway track infrastructure has led to an increase in the number of properties affected by ground-borne railway vibrations [15–19]. The negative effects caused by railway traffic are more prominent in the presence of local irregularities [20] and are addressed in international standards [21–23]. Thus, it is desirable to estimate the potential increase in vibrations levels in nearby buildings.

To do so, a variety of numerical models have been proposed to compute building induced vibrations due to railway traffic. Prior to the construction stage of a new railway project or the construction of a building near an existing line, a detailed design is required [23] possibly using comprehensive 3D models with high computational cost. These include Fiala et al. [24] who developed a comprehensive BEM-FEM model to calculate building vibration and indoor noise. Alternatively, Galvín et al. [25] presented a coupled train–track–soil-structure 3D BEM-FEM model formulated in the time domain where nonlinear behaviour of structures could be also considered. Moreover, the problem of vibration in bridges was studied by comprehensive models [26, 27]. Coulier et al. [28] studied the source (track) and receiver (building) interaction in order to determine the uncertainty of using uncoupled approaches. It was concluded that for a ballasted track the assumption of uncoupling was acceptable for distances from the track greater than six times the Rayleigh wave length.

Uncoupled simplified procedures are normally used at an earlier stage of railway line development [23].

These represent useful tools, because their lower computation times. Two such methods to evaluate building vibrations due to a train passage have been proposed by the Federal Railroad Administration (FRA) and the Federal Transit Administration (FTA) of the U.S. Department of Transportation [29–31]. Rücker et al. [32] developed a simplified prediction tool that allows to evaluate free-field and building vibrations. Auersch [33] analysed building vibration in inhomogeneous soils and proposed a simplified methodology to consider SSI in a layered ground. He studied building induced vibrations using a simple soil-wall-floor model based on an empirical transfer function obtained from the characteristics of the structure [34]. Moreover, this also included with a simple method to estimate vibration in buildings on pile foundations [35]. Hussein et al. [36] developed a sub-modelling method where a train-track-soil 3D model was coupled with a 2D building approach based on beam elements. Also, this presented a 3D model to calculate vibration in a building based on pile-foundation by railway traffic in a nearby underground tunnel [37]. Later, Kouroussis et al. [38] proposed a decoupled FE model to predict building vibrations due to tramway traffic with local irregularities. Also a hybrid numerical/experimental model to assess ground and building vibration was presented [39, 40]. In this a vehicle-track numerical approach which simulated vibration generation due to a variety of railroad artefacts was combined with a experimental procedure based on multiple single source transfer mobilities that modelled the transmission mechanism between rail and nearby structures. Lopes et al. [41, 42] developed an uncoupled model to evaluate building vibrations induced by railway traffic in tunnels. Free-field response was computed using a 2.5 D FEM-Perfectly Matched Layers (PML) model and combined with a 3D FEM model to evaluate the building response. Connolly et al. [43, 44] proposed a scoping model to predict vibrations and in-door noise in buildings due to railway traffic. A wide range of soil vibration records generated by a 3D FEM model was used to build a machine learning approach. This procedure was combined with empirical factors [31] to compute building vibrations. López-Mendoza et al. [45] presented a scoping model based on modal superposition analysis. The free-field vibration was discretised into the frequency range corresponding to the modes of the structure. Kuo et al. [46] presented a hybrid model that combined recorded data and numerical predictions considering the definitions proposed by the FRA [31]. The source, propagation and receiver mechanisms were uncoupled. Recently Connolly et al. [47] presented a decoupled procedure to analyse soil-building vibrations due to railway irregularities. A 2.5D time-frequency domain model to compute soil vibrations was combined with a 3D FEM procedure to obtain building vibrations induced by railway defects.

This paper uses a simple procedure where the source (ground motion) and the receiver (building) are uncoupled. It is focused on the receiver model and proposes soil-structure transfer functions considering SSI. These soil-structure transfer functions are combined with free-field vibrations to compare building vibration with low computational effort. The model is numerically verified comparing with a comprehensive BEM-FEM model. Finally, the proposed model is used to analyse building vibrations due to local irregularities.

2. Methodology

ISO 14837-1 standard [23] defines the magnitude of building vibration $A(f)$ in the frequency domain f as a function that the source $S(f)$, the propagation $P(f)$ and the receiver $R(f)$. Considering the assumption that all the three terms are uncoupled (Figure 1), the magnitude of the building vibration $A(f)$ can be expressed as:

$$A(f) = S(f)P(f)R(f) \tag{1}$$

The procedure developed by the Federal Railroad Administration (FRA) [31] to estimate building response

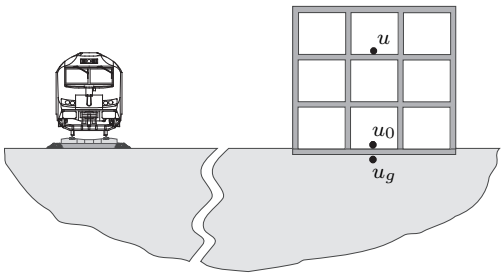

Figure 1: Scheme of decoupled model.

due to railway traffic proposes two factors influencing the receiver: 1) the floor-to-floor attenuation, and, 2) the amplification due to the resonance of floors, walls and ceilings. The present work includes these factors defining the floor amplification F_a as the increment in the building response u with respect to the foundation response u_0 (Figure 1). The floor amplification is computed as:

$$F_a(f) = u(f)/u_0(f) \tag{2}$$

Also, the effect of the building foundation should be considered using the coupling loss C_l [31]. The coupling loss is related with the soil-foundation interaction. This consits in the ratio between the building foundation response u_0 and the free-field vibration u_g (Figure 1). In this work, the coupling is evaluated as:

$$C_l(f) = u_0(f)/u_g(f) \tag{3}$$

The following expression to calculate the building response u can be obtained by combining Equations (2) and (3):

$$u(f) = F_a(f)C_l(f)u_g(f) \tag{4}$$

Comparing Equations (1) and (4), it can be seen that the source $S(f)$ and the propagation $P(f)$ terms are included in the free-field vibration u_g, whereas the receiver term $R(f)$ is part of the floor amplification

F_a and the coupling loss C_l. The main novelty of this work is applying the soil-structure transfer functions $u/u_g = F_a(f)C_l(f)$ depending only on the receiver, to predict building vibration by railway traffic. The soil-structure transfer function represents the building response due to a displacement impulse applied at the building foundation. A key advantage of this approach is the computational efficiency arrising because the soil-structure transfer function is computed only once for a soil-building subsystem and later it is combined with a wide range of free-field vibration data to analyse multiple scenarios. These low requirements mean the approach is well-suited to early stage railway projects. On the other hand, although this work is focused on the application of soil-structure transfer functions to assess building vibrations by railway traffic, these soil-structure transfer functions can be used to predict building vibration due to diverse sources (e.g. construction, earthquake, road traffic, blast) where the free-field vibration spectrums is known.

This work uses the methodology presented in Reference [47] to model the source-propagation subsystem $(S(f),\ P(f))$. Once it is solved for the source-propagation subsystem, it can be used to compute the building vibration $A(f)$. To do so, the building foundation is excited by the free-field response u_g. The SSI is integrated in the proposed methodology using a simplified method. Below, it will be related the procedure to model the receiver soil-structure subsystem $(R(f))$.

2.1. Simplified building-soil coupling model

The simplified method is a 3D time domain FEM model. The dynamic equilibrium equation of a structure can be written as:

$$\mathbf{M}\ddot{\mathbf{u}}(t) + \mathbf{C}\dot{\mathbf{u}}(t) + \mathbf{K}\mathbf{u}(t) = \mathbf{F} \tag{5}$$

where $\mathbf{M}$, $\mathbf{C}$ and $\mathbf{K}$ are the mass, damping and stiffness matrices, respectively. $\mathbf{u}(t)$, $\dot{\mathbf{u}}(t)$, and $\ddot{\mathbf{u}}(t)$ are the building displacement, velocity and acceleration, respectively, while $\mathbf{F}$ represents the external force. The FEM equation is solved at each time step following an implicit time integration GN22 Newmark method [48, 49]. Structural damping is considered following a Rayleigh model [50], where the damping matrix $\mathbf{C}$ is proportional to the the mass $\mathbf{M}$ and stiffness $\mathbf{K}$ matrices as $\mathbf{C} = d_m\mathbf{M} + d_k\mathbf{K}$. Constants d_m and d_k are chosen depending on the modal damping of the structure.

Next a brief description of the simplified methodology to model SSI focused on the case of a building with a slab foundation on the surface of a homogeneous soil is presented. The foundation consisting of a slab. A drawback of the approach is that it can not be applied to deep foundations. In order to consider SSI for layered soils, equivalent homogeneous soils are obtained depending on the average shear wave velocity V_{s30} as defined in Eurocode 8 [51], and computed as:

$$V_{s30} = \frac{30\ [\mathrm{m}]}{\sum_i^{N_s} \frac{h_i}{c_{s_i}}} \tag{6}$$

where h_i is the thickness of the i th layer, N_s the total number of layers in the top 30 m and c_{s_i} the shear

wave velocity of the ith layer. Therefore, equivalent homogeneous soils with $c_s = V_{s30}$ are considered to model layered soils.

The simplified method is based on recommendations from the National Institute of Standards and Technology (NIST) [52]. This proposes to integrate SSI by adding spring-damper elements to the foundation of the building. As the building is not embedded in the soil, expressions to define horizontal spring-damper elements are discarded. The formulation to calculate vertical spring-damper elements is below.

To explain the simplified model, consider a rectangular building with floor plan dimensions $2L \times 2B$, where $L \geq B$ (Figure 2). Note that in the following formulation, the sub-indices x, y and z are related to the translation along the respective axis. Also the sub-indices xx and yy refer the rocking about the x and y respectively, whereas sub-index zz is related to the torsion about the z axis (Figure 2). Hereafter, the formulation considers the x axis to be the largest dimension of the foundation ($2L$).

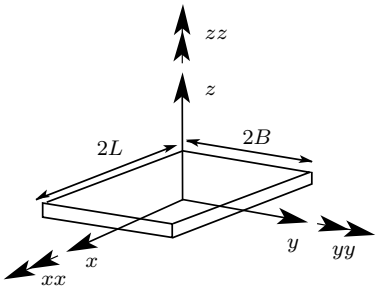

Figure 2: Scheme of the plan geometry of the building foundation.

A spring-damper system is added to the foundation allowing it to be modelled as rigid or flexible. For the rigid case, a single spring-damper element defined by its stiffness k_z and the dashpot coefficient c_z. On the other hand, flexible foundations are simulated using spring-damper elements (k_z^i , c_z^i) spread across the foundation area, where k_z^i and c_z^i are the properties of the i^{th} spring-damper element.

2.1.1. Rigid foundation

If the foundation is rigid, it can be represented by a single spring-damper element (k_z , c_z). The vertical stiffness of the full system k_z, is evaluated using the formulation presented in Reference [53]:

$$k_z = K_{z,surf}\alpha_z \tag{7}$$

where $K_{z,surf}$ is the vertical static stiffness of the surface foundation and α_z is the dynamic stiffness modifier. The vertical static stiffness $K_{z,surf}$ is obtained from the shear modulus G and Poison's ratio of the soil ν, and the foundation dimensions L and B, using:

$$K_{z,surf} = \frac{GB}{1-\nu}\left(3.1\left(\frac{L}{B}\right)^{0.75} + 1.6\right) \tag{8}$$

Also the dynamic stiffness modifier α_z depends on the structural properties and is evaluated as:

$$\alpha_z = 1 - \frac{\left(0.4 + \frac{0.2}{\frac{L}{B}}\right) a_0^2}{\frac{10}{1+3\left(\frac{L}{B}-1\right)} + a_0^2} \tag{9}$$

where a_0 is the dimensionless frequency computed from the S-wave velocity c_s and the angular frequency of the first bending mode ω_1 (discarding SSI), as:

$$a_0 = \frac{\omega_1 B}{c_s} \tag{10}$$

Once the vertical stiffness k_z is obtained, the dashpot coefficient of the full foundation c_z can be computed using [52]:

$$c_z = 2k_z \frac{\beta_z + \beta_s}{\omega_1} \tag{11}$$

where β_s is the damping ratio of the soil and β_z is the radiation damping ratio obtained as [53]:

$$\beta_z = \frac{4\psi\frac{L}{B}}{\frac{K_{z,surf}}{GB}} \frac{a_0}{2\alpha_z} \tag{12}$$

where $\psi = \sqrt{2\left(1-\nu\right)\left(1-2\nu\right)}$, limited to $\psi \leq 2.5$.

Following the same procedure to calculate the vertical stiffness k_z (Eq. (7)), the rocking stiffness can be obtained as [53]:

$$k_{yy} = K_{yy,surf}\alpha_{yy} \qquad k_{xx} = K_{xx,surf}\alpha_{xx} \tag{13}$$

The rocking static stiffnesses ($K_{xx,surf}$, $K_{yy,surf}$) and the dynamic stiffness modifiers (α_{xx}, α_{yy}) are evaluated as:

$$K_{yy,surf} = \frac{GB^3}{1-\nu}\left(3.73\left(\frac{L}{B}\right)^{2.4} + 0.27\right) \qquad K_{xx,surf} = \frac{GB^3}{1-\nu}\left(3.2\left(\frac{L}{B}\right) + 0.8\right) \tag{14}$$

$$\alpha_{yy} = 1 - \frac{0.55a_0^2}{0.6 + \frac{1.4}{\left(\frac{L}{B}\right)^3} + a_0^2} \qquad \alpha_{xx} = 1 - \frac{\left(0.55 + 0.01\sqrt{\frac{L}{B}-1}\right) a_0^2}{2.4 - \frac{0.4}{\left(\frac{L}{B}\right)^3} + a_0^2} \tag{15}$$

In the same way as for the vertical dashpot (Eq. (11)), the rocking dashpot is computed as [53]:

$$c_{yy} = 2k_{yy}\frac{\beta_{yy} + \beta_s}{\omega_1} \qquad c_{xx} = 2k_{xx}\frac{\beta_{xx} + \beta_s}{\omega_1} \tag{16}$$

where the radiation damping ratios β_{xx} and β_{yy} are calculated as:

$$\beta_{yy} = \frac{\frac{4\psi}{3}\left(\frac{L}{B}\right)^3 a_0^2}{\frac{K_{yy,surf}}{GB^3}\left(\frac{1.8}{1+1.75\left(\frac{L}{B}-1\right)} + a_0^2\right)} \frac{a_0}{2\alpha_{xx}} \qquad \beta_{xx} = \frac{\frac{4\psi}{3}\frac{L}{B}a_0^2}{\frac{K_{xx,surf}}{GB^3}\left(2.2 - \frac{0.4}{\left(\frac{L}{B}\right)^3} + a_0^2\right)} \frac{a_0}{2\alpha_{yy}} \tag{17}$$

2.1.2. Flexible foundation

Equations 7 and 11 compute the spring-damper element (k_z, c_z) properties for rigid foundations. However, in order to consider the effect of a flexible foundation, the NIST proposes smeared spring and damper elements. To do so, the vertical values k_z and c_z are normalized by the foundation area to obtain the stiffness intensity $\tilde{k}_z^i = k_z/4BL$ and dashpot intensity $\tilde{c}_z^i = c_z/4BL$. Then, the stiffness k_z^i and dashpot c_z^i of a vertical spring-damper element in the interior of the foundation can be computed as:

$$k_z^i = \tilde{k}_z^i dA^i \qquad c_z^i = \tilde{c}_z^i dA^i \tag{18}$$

where dA^i is the individual area for the i^{th} spring-damper element (Figure 3).

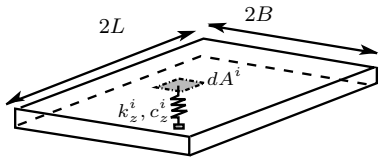

Figure 3: Individual area dA^i for the i spring-damper element.

If these expressions (Eq. (18)) are used across the full foundation, the rotational stiffness would be underestimated and the rotational damping would be overestimated [52]. To correct these effects, factors R_k and R_c are applied to the spring-damper elements along a strip area on the the foundation edge. To do so, the stiffness and damping of a vertical spring-damper element at the foundation edge are estimated as:

$$k_z^i = R_k \tilde{k}_z^i dA^i \qquad c_z^i = R_c \tilde{c}_z^i dA^i \tag{19}$$

The width of the foundation edge strip is computed from the foundation end ratio R_e as $R_e L$ and $R_e B$ for the x and y axes, respectively. A value in the range from 0.3 to 0.5 is usually selected for the foundation end ratio R_e. In this work an end ratio $R_e = 0.5$ is used. Figure 4 shows the spring-damper element properties (k_z^i, c_z^i) depending on the position of the i^{th} element across the foundation.

Regarding the estimation of the correction factors R_k and R_c, the following expressions are proposed by the NIST:

$$R_{k,yy} = \frac{\frac{3k_{yy}}{4\tilde{k}_z^i BL^3} - (1-R_e)^3}{1-(1-R_e)^3} \qquad R_{k,xx} = \frac{\frac{3k_{xx}}{4\tilde{k}_z^i B^3 L} - (1-R_e)^3}{1-(1-R_e)^3} \tag{20}$$

$$R_{c,yy} = \frac{\frac{3c_{yy}}{4\tilde{c}_z^i BL^3}}{R_{k,yy}\left(1-(1-R_e)^3\right)+(1-R_e)^3} \qquad R_{c,xx} = \frac{\frac{3c_{xx}}{4\tilde{c}_z^i BL^3}}{R_{k,xx}\left(1-(1-R_e)^3\right)+(1-R_e)^3} \tag{21}$$

where k_{xx} and k_{yy} are the rotational stiffnesses about the x and y axes respectively, considering a rigid foundation. Also the dashpot coefficients c_{xx} and c_{yy} represent the rotational damping about the x and y

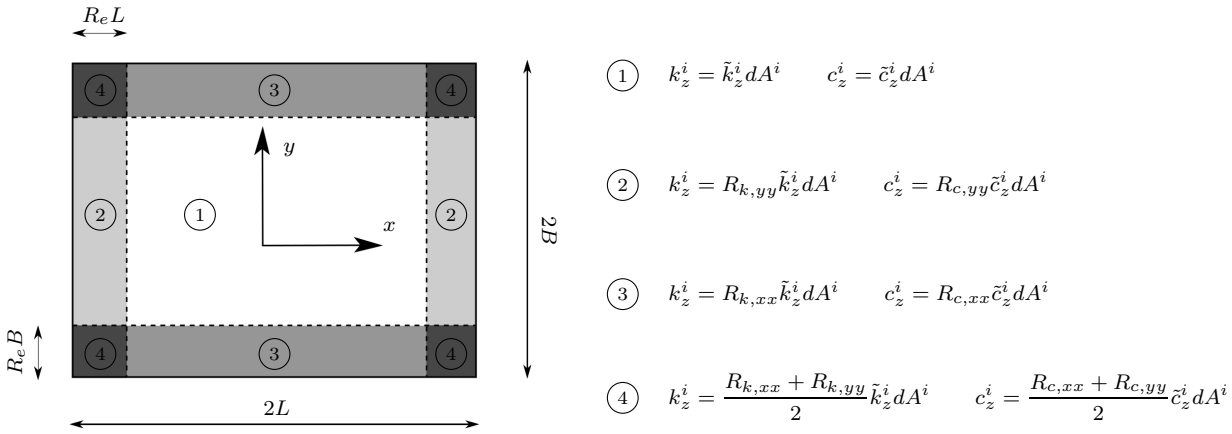

Figure 4: Spring-damper element properties across the foundation.

axes respectively.

2.2. Methodology summary

1. The spring-damper system applied to the building foundation are computed depending on the following inputs: the soil properties (c_s, G, ν, β_s), the foundation dimension (B, L) and the first bending mode (ω_1).
2. These inputs allow to obtain the spring-damper system properties for a rigid foundation (Equations (7) and (11)) or a flexible foundation (Equations (18) and (19)).
3. The spring-damper system is assembled to building model constructing the mass, damping and stiffness matrices ($\mathbf{M}$, $\mathbf{C}$, $\mathbf{K}$).
4. The soil-structure transfer function $u/u_g = F_a(f)C_l(f)$ is computed solving the dynamic equilibrium equation of a structure due to a displacement impulse applied at the building foundation (Equation (5)).
5. Soil-structure transfer function is combined with free-field vibration u_g [47] to obtain building response u by railway traffic (Equation (4)).

3. Building-soil model validation

In this section, the dynamic behaviour of three buildings are compared with those obtained from the `SSIFiBo` toolbox [54]. The `SSIFiBo` toolbox represents a comprehensive model based on a 3D time domain BEM-FEM methodology. The solution u^r represents the building response from `SSIFiBo` toolbox, hereafter called the 'reference' solution, whereas u^s is the solution computed using the simplified method considering flexible foundation. A third solution is also computed for each case, where SSI $\tilde{u}$ is ignored.

To quantify the effect of SSI, it is studied using the ratios:

$$\Delta u^r(f) = \frac{u^r(f)}{\tilde{u}(f)} \qquad \Delta u^s(f) = \frac{u^s(f)}{\tilde{u}(f)} \tag{22}$$

Substituting Equation (4) into Equation (22) and remembering that the coupling loss $\tilde{C}_l$ for the solution without SSI is equal to 1, the SSI effect can be rewritten as:

$$\Delta u^r = C_l^r F_a^r / \tilde{F}_a \qquad \Delta u^s = C_l^s F_a^s / \tilde{F}_a \tag{23}$$

This work analyses the assumption that SSI depends only on the coupling loss $\Delta u^r \approx C_l^r$ and $\Delta u^s \approx C_l^s$. Substituting this simplification in Equation (23) involves that the solution ignoring SSI presents floor amplifications close to those obtained using the reference model $F_a^r/\tilde{F}_a \approx 1$ and the simplified method $F_a^s/\tilde{F}_a \approx 1$. This assumption allows for the analysis of two simplified solutions u^I and u^{II}, where the coupling loss is computed using the reference C_l^r and the simplified C_l^s models, respectively.

Therefore, to summarise, the following solutions are analysed in this work:

$$\begin{aligned}
u^r(f) &= F_a^r(f) C_l^r(f) u_g(f) \\
u^s(f) &= F_a^s(f) C_l^s(f) u_g(f) \\
\tilde{u}(f) &= \tilde{F}_a(f) u_g(f) \\
u^I(f) &= \tilde{F}_a(f) C_l^r(f) u_g(f) \\
u^{II}(f) &= \tilde{F}_a(f) C_l^s(f) u_g(f)
\end{aligned}$$

The analysis of the buildings excited due to an incident wavefield allows for the evaluation of the accuracy of the simplified method (Section 2.1) and the assumption described above.

The three types of building consist of four, six and twelve storey concrete buildings founded on a slab, with framed walls (Figure 5). Floor plan dimensions of 12m × 40m, 20m × 20m and 12m × 12m are considered for the four, six and twelve storey buildings, respectively. The floors are simply supported concrete slabs. Four edge beams are considered in the twelve storey building. The concrete material has the following properties: Young's modulus $E = 20 \times 10^9\,\mathrm{N/m^2}$, Poisson's ratio $\nu = 0.2$ and density $\rho = 2400\,\mathrm{kg/m^3}$. A structural damping, $\zeta = 5\,\%$ is set for the dominant mode shapes (Figure 6). The structures are discretised using two-node Euler-Bernoulli elements to represent columns and beams and four-node shell elements for the floors and the framed walls. Table 1 summarises the building properties.

The dominant bending mode shapes computed without considering SSI can be observed in Figure 6.

The buildings are on a homogeneous soil with P-wave velocity $c_p = 250\,\mathrm{m/s}$, S-wave velocity $c_s = 100\,\mathrm{m/s}$, material damping $\xi = 0.06$ and density $\rho = 1750\,\mathrm{kg/m^3}$. The building responses are presented for the observation points A and B (Figure 5).

The incident wave field consists of a uniform vertical displacement $\tilde{\mathbf{u}}_g = \delta(t)$ m, where δ is the Dirac delta function. Therefore, the incident wave field in the frequency domain presents a constant value. This incident

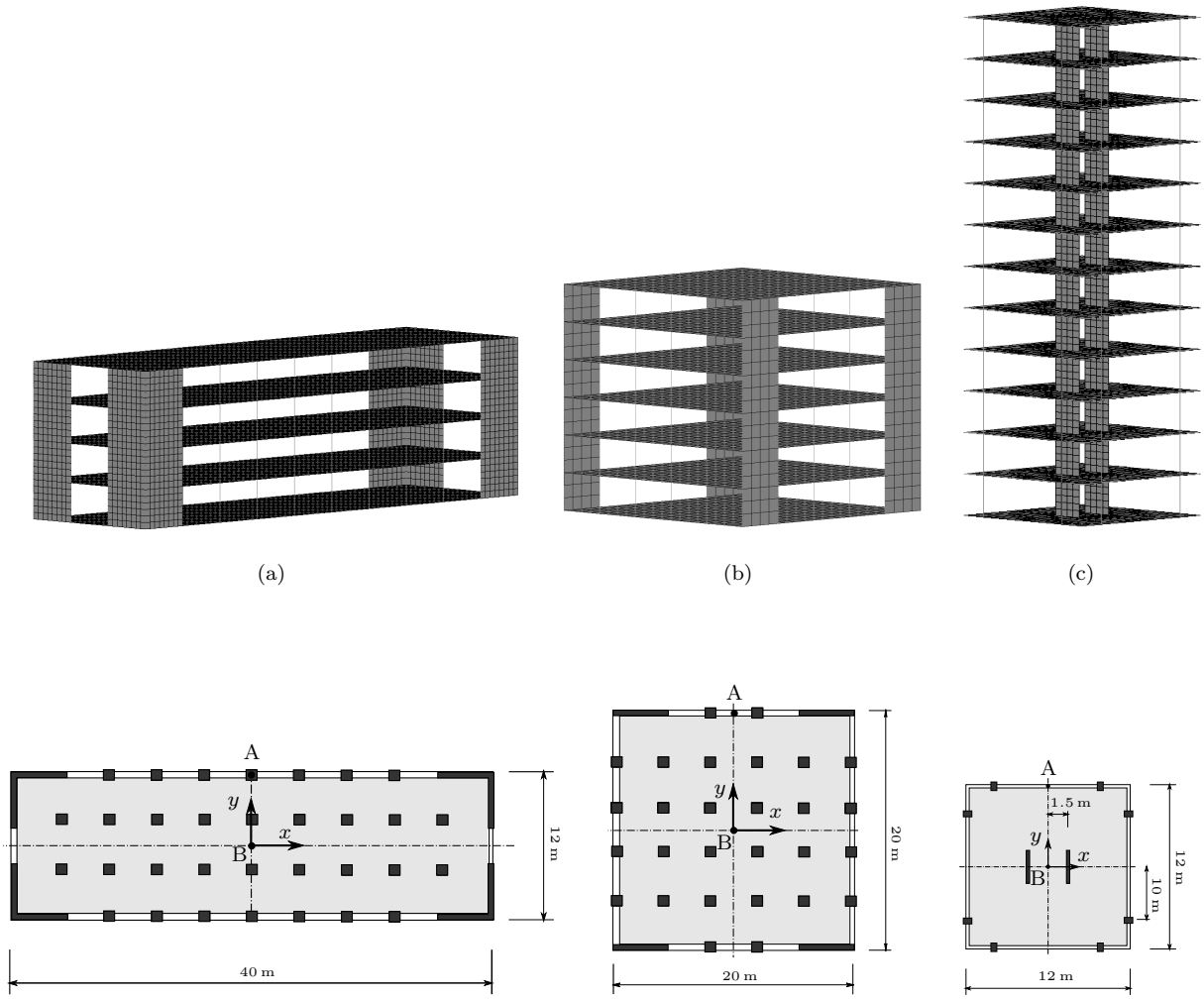

Figure 5: Discretization and plan geometry of the (a, d) four, (b, e) six and (c, f) twelve-storey buildings.

Table 1: Building properties.

	4-storey	6-storey	12-storey
Column section $[\mathrm{m}^2]$	0.3×0.3	0.3×0.3	0.6×0.4
Edge beam section $[\mathrm{m}^2]$	–	–	0.6×0.2
Frame wall thickness [m]	0.25	0.25	0.15
Floor slab thickness [m]	0.25	0.25	0.2
Foundation slab thickness [m]	0.5	1	1

wave field allows for the calculation of the building response solely in terms of the receiver $u(f) = F_a(f)C_l(f)$ (Equation (4)). Also the coupling loss represents the foundation response $C_l(f) = u_0(f)$ (Equation (3)).

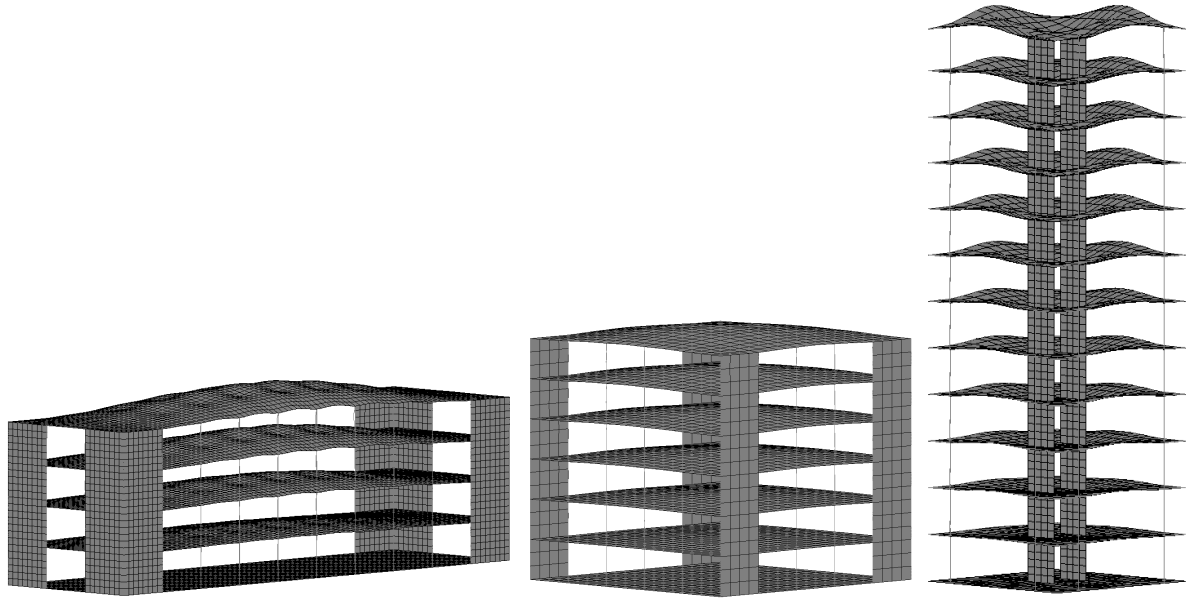

(a) Mode at 9.5 Hz (b) Mode at 6.9 Hz (c) Mode at 9.1 Hz

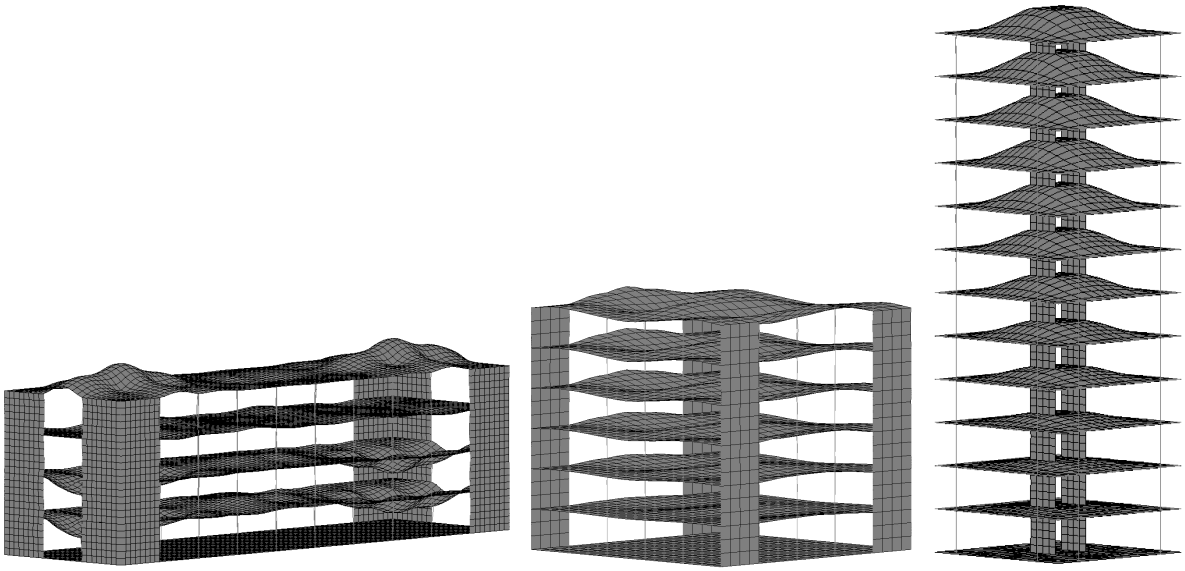

(d) Mode at 17.8 Hz (e) Mode at 14.2 Hz (f) Mode at 20.1 Hz

Figure 6: Dominant bending mode shapes of the (a,d) four-storey building, (b,e) and (c,f) twelve-storey building.

Figure 7 shows the one-third octave band representation [55] of the coupling loss computed using the reference model and the simplified method. Overall it is seen that the presence of the building attenuates the soil vibration, while the simplified method presents an acceptable estimation of the coupling loss. Moreover, the coupling loss does not depend strongly on the type of building or the observation point.

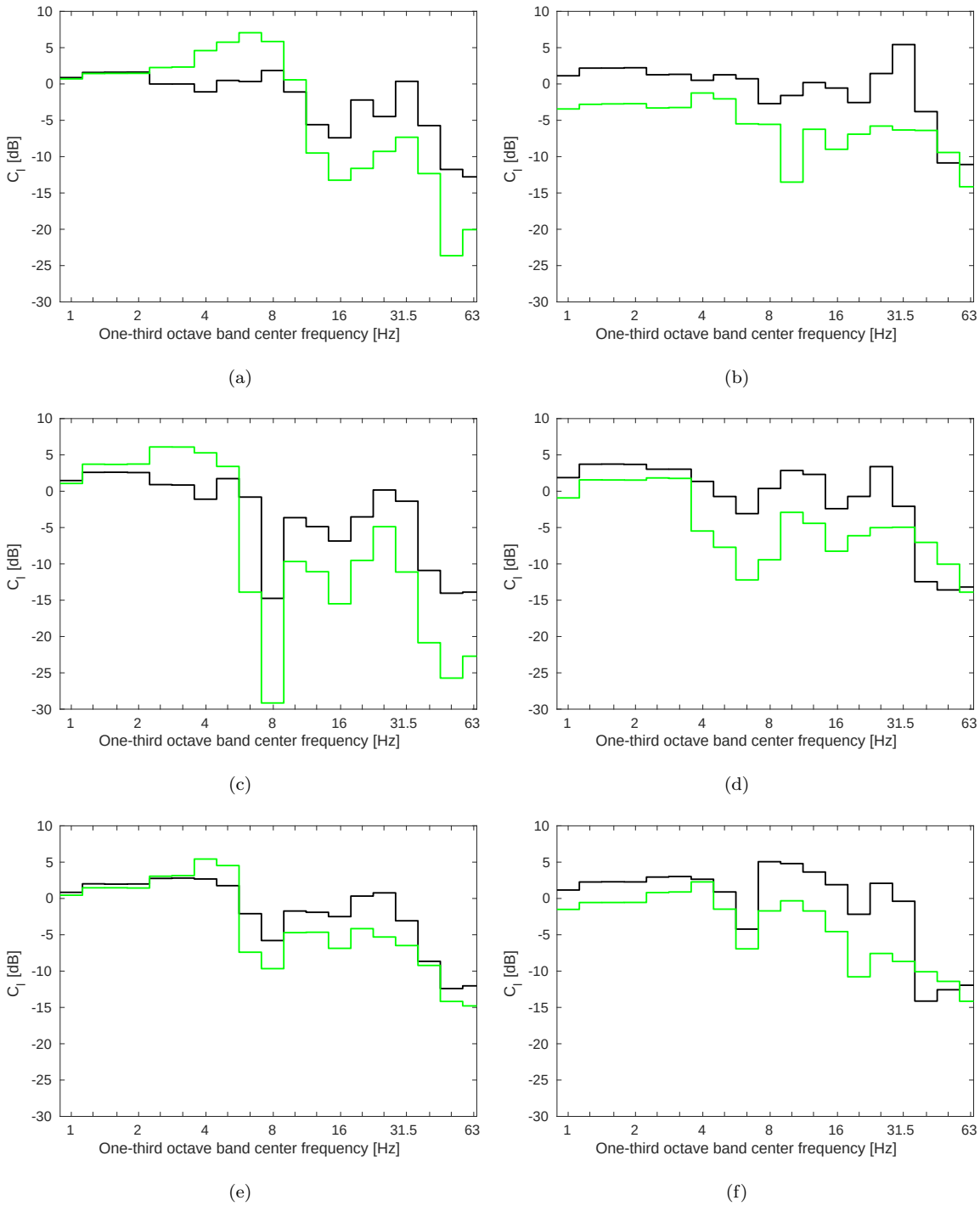

Figure 7: One-third octave band center frequency of the coupling loss due to an incident wave field, at the observation points (a,c,e) A and (b,d,f) B of the (a,b) four-storey, (c,d) six-storey and (e,f) twelve-storey buildings, from the (black line) `SSIFiBo` toolbox and the (green line) simplified methodology.

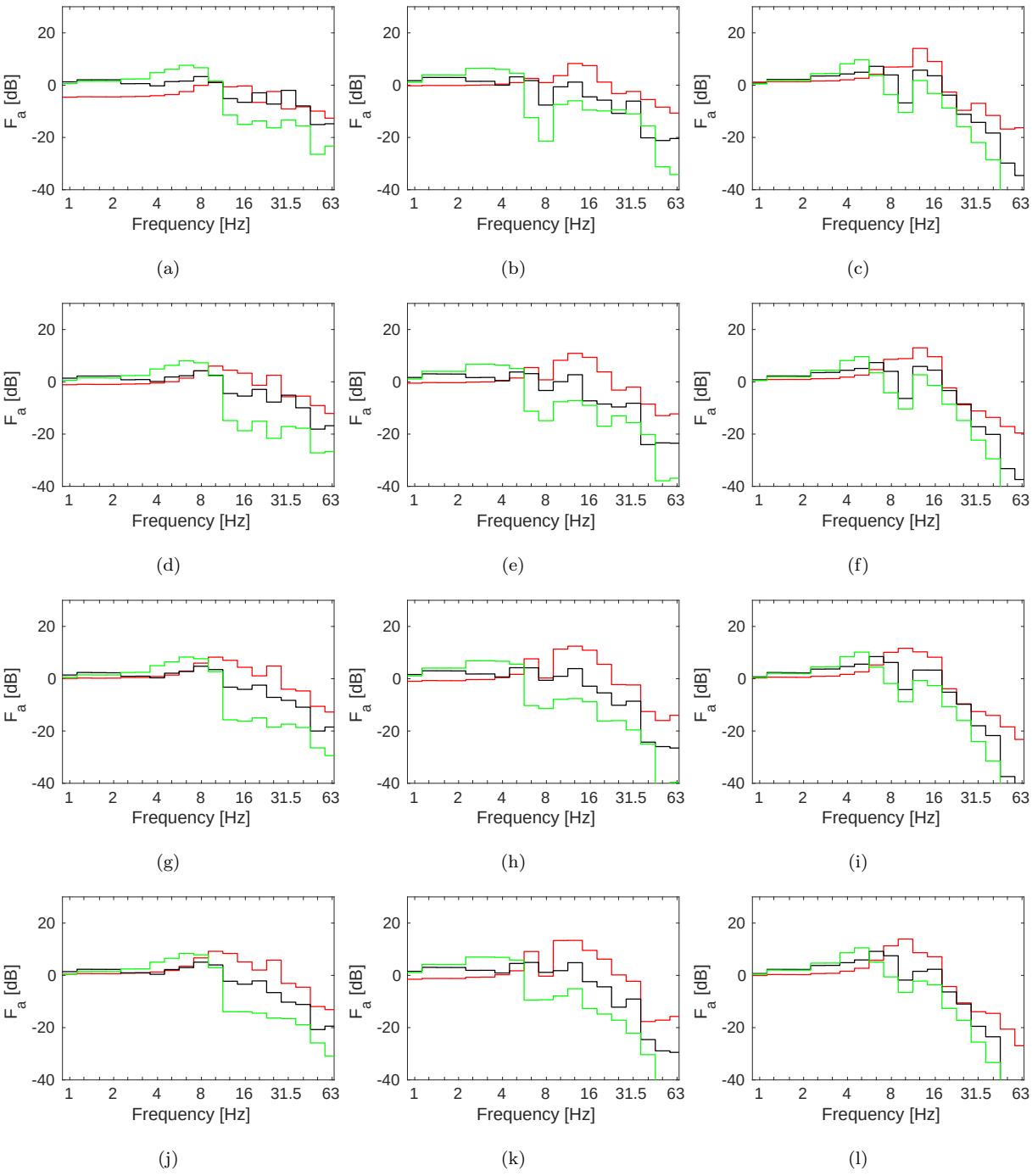

Figure 8: One-third octave band center frequency of the floor amplification due to an incident wave field, at the observation point A of the (a,d,g,j) four-storey, (b,e,h,k,) six-storey and (c,f,i,l) twelve-storey buildings, at the (a,b,c) first, (d,e,f) second, (g,h,i) third and (j,k,l) fourth floors, from the (black line) `SSIFiBo` toolbox , the (green line) simplified methodology and (red line) ignoring SSI.

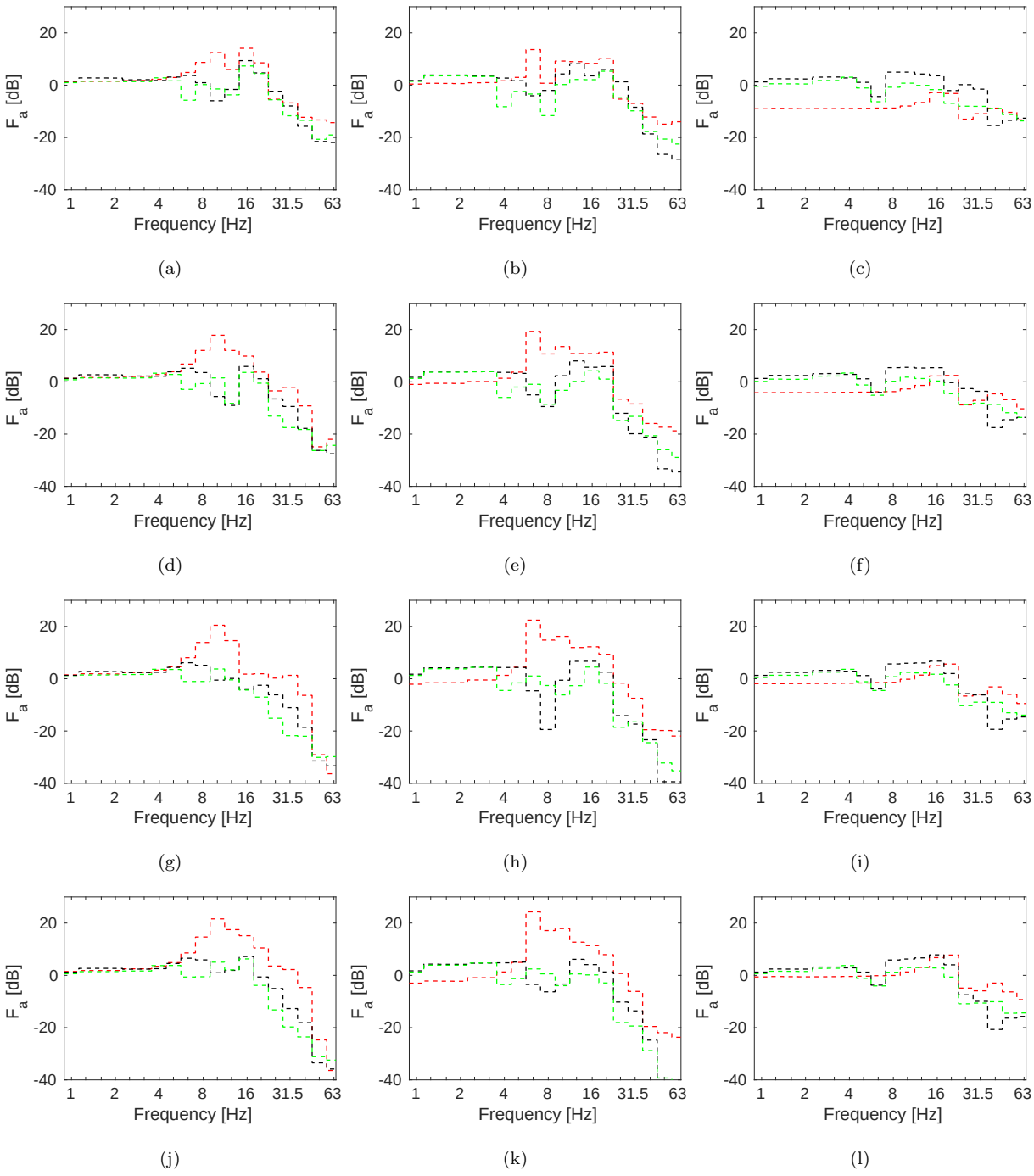

Figure 9: One-third octave band center frequency of the floor amplification due to an incident wave field, at the observation point B of the (a,d,g,j) four-storey, (b,e,h,k,) six-storey and (c,f,i,l) twelve-storey buildings, at the (a,b,c) first, (d,e,f) second, (g,h,i) third and (j,k,l) fourth floors, from the (black line) `SSIFiBo` toolbox , the (green line) simplified methodology and (red line) ignoring SSI.

The floor amplification (Equation 2) is shown in Figures 8 and 9 from the first to fourth floors, for the simplified and reference models, and the case of ignoring SSI. Overall the floor amplification increases with the storey level in the low frequency range, while the excitation is filtered at higher frequencies according to the modal parameters of the buildings. It is seen that the floor amplification of each storey level is within the same order of magnitude. Although the simplified methodology presents a better agreement with the reference model results, the response from the solution ignoring SSI $\tilde{F}_a$ also matches acceptably well.

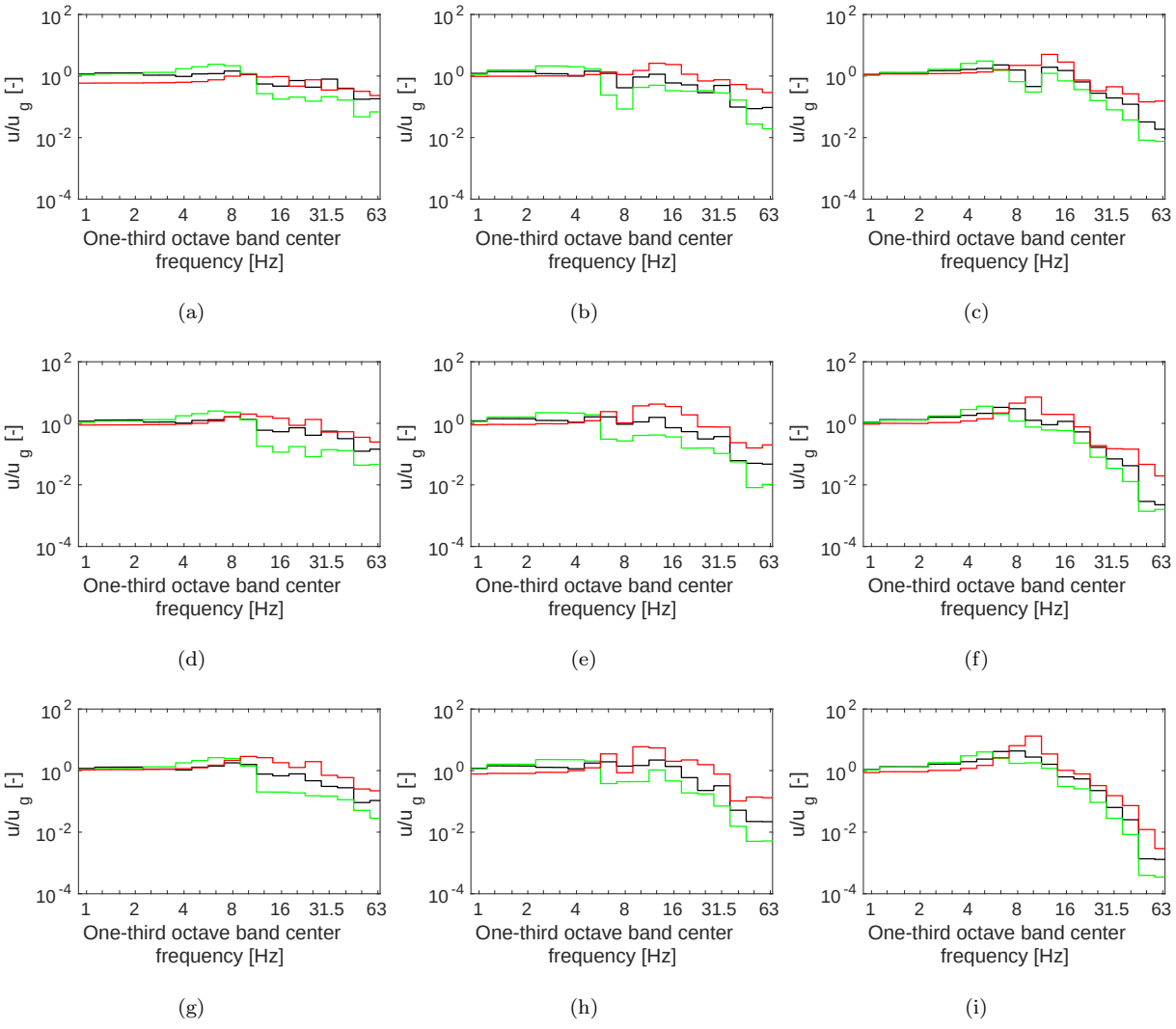

Figure 10: One-third octave band center frequency of the soil-structure transfer function due to an incident wave field, at the observation point A of the (a,d,g) four-storey, (b,e,h) six-storey and (c,f,i) twelve-storey buildings, at the (a,b,c) first, (d,e,f) middle and (g,h,i) top floors, from the (black line) `SSIFiBo` toolbox, the (green line) simplified methodology and (red line) ignoring SSI.

Figures 10 and 11 present the soil-structure transfer function $u(f)/u_g(f)$ for all 3 models. This soil-

structure transfer function is obtained from the receivers terms $u(f)/u_g(f) = F_a(f)C_l(f)$ (Equation (4)). It can be concluded that the shape and magnitude of the response from the simplified method match reasonable well with those obtained from the reference model, although the results from the simplified method are underestimated. The response ignoring SSI overestimates the result.

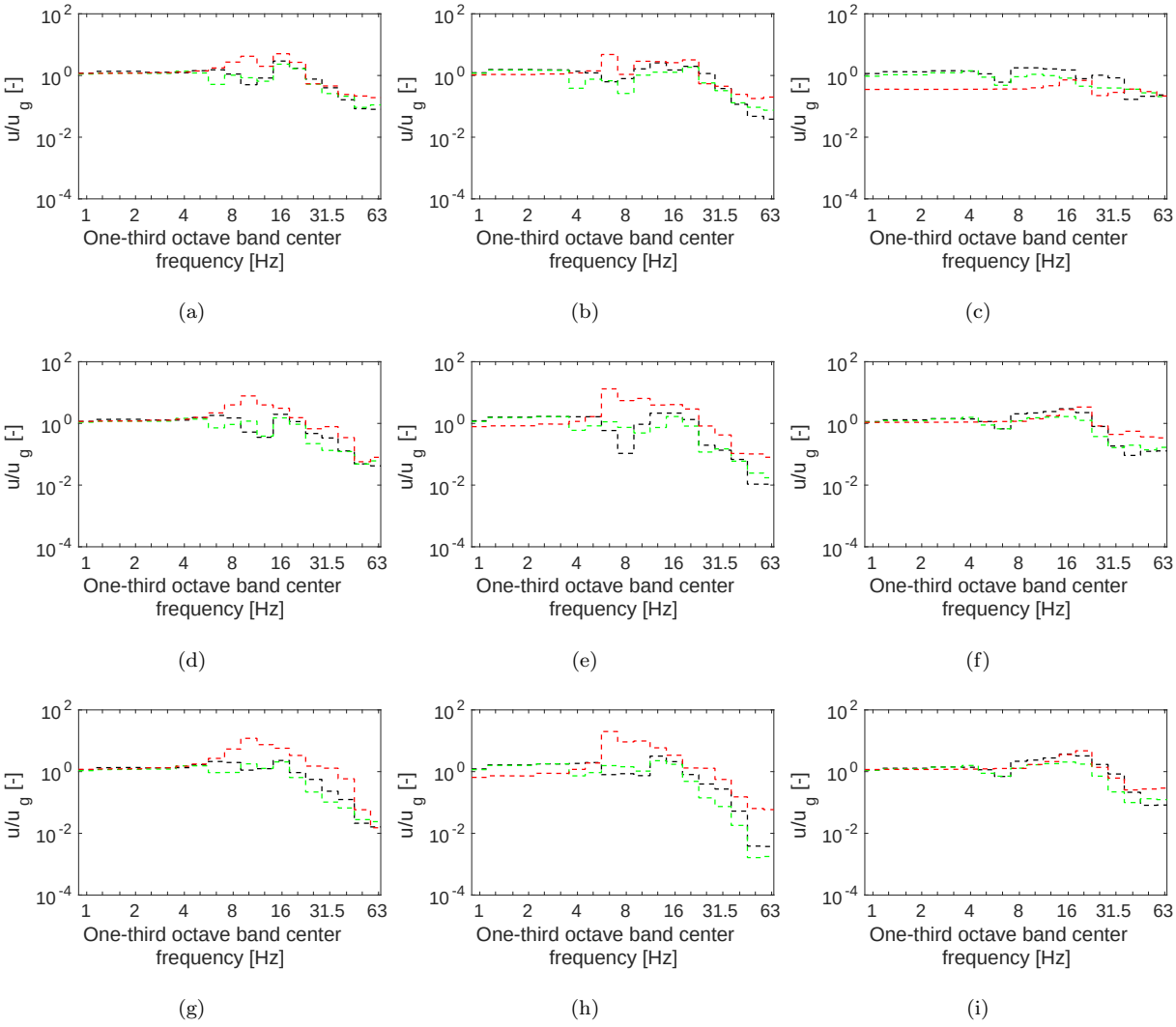

Figure 11: One-third octave band center frequency of the soil-structure transfer function due to an incident wave field, at the observation point B of the (a,d,g) four-storey, (b,e,h) six-storey and (c,f,i) twelve-storey buildings, at the (a,b,c) first, (d,e,f) middle and (g,h,i) top floors, from the (black line) `SSIFiBo` toolbox, the (green line) simplified methodology and (red line) ignoring SSI.

The effect of SSI is shown in Figure 12 which displays the ratios Δu^r and Δu^s (Equation (22)) for all the storey levels of the buildings. Also, it superimposes the coupling loss factors C_l^r and C_l^s to evaluate the accuracy of the approximations $\Delta u^r \approx C_l^r$ and $\Delta u^s \approx C_l^s$, defined above. Although there are amplifications

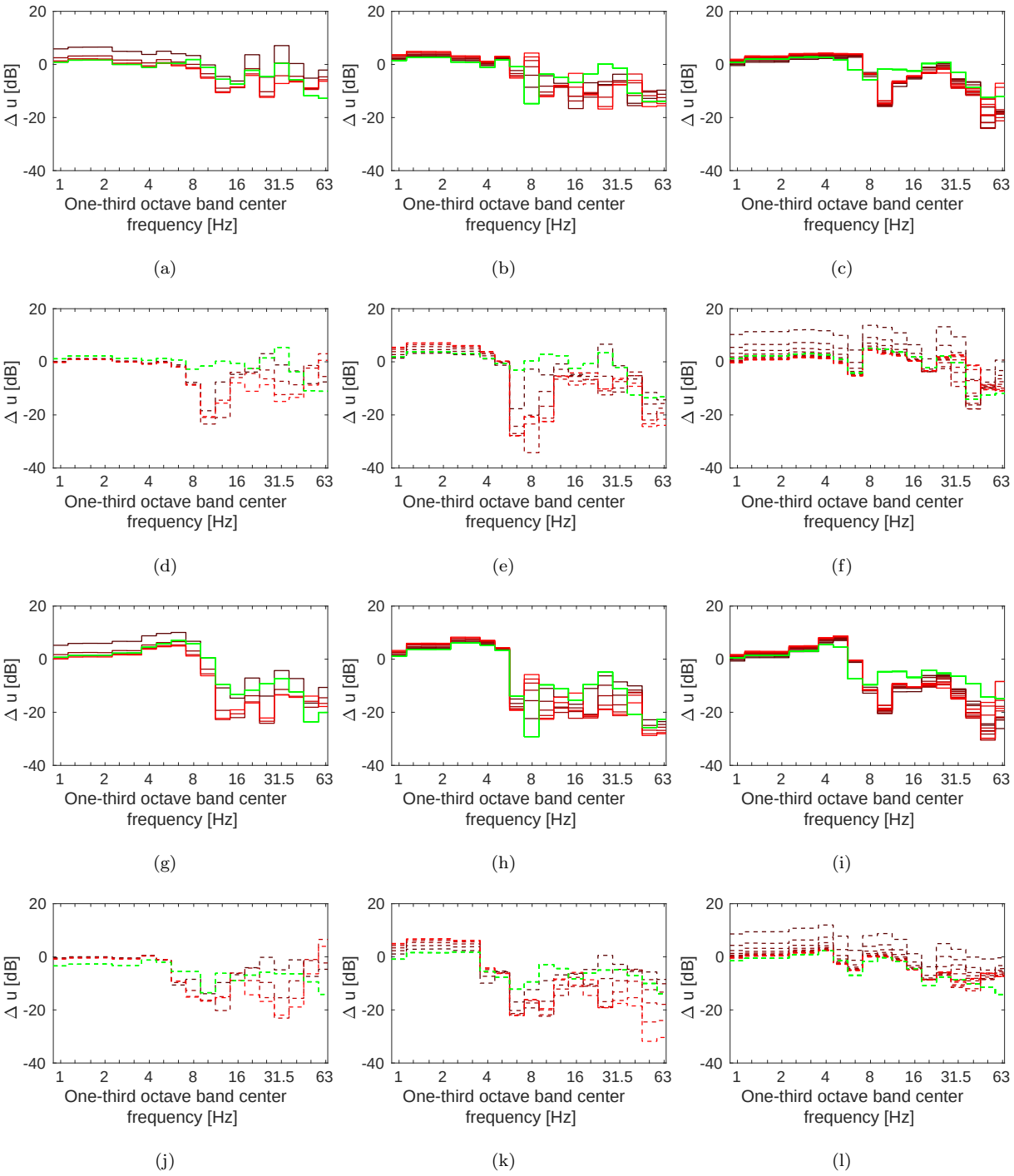

Figure 12: One-third octave band center frequency of the (solid line) ratios (a-f) Δu^r and (g-l) Δu^s at the observation points (a,b,c,g,h,i, solid line) A and (d,e,f,j,k,l, dashed line) B of the (a,d,g,j) four-storey, (b,e,h,k) six-storey and (c,f,i,l) twelve-storey buildings. SSI attenuation from the (darkest line) first floor to the (red line) top floor. Superimposed is the (green line) coupling loss computed from the (a-f) `SSIFiBo` toolbox and the (g-l) simplified method.

at low frequencies, it can be seen that there are attenuations at mid and high frequencies due to SSI. It is observed that the effect of SSI depends minorly on storey level. However, it is valid to approximate the SSI effect using the coupling loss factor.

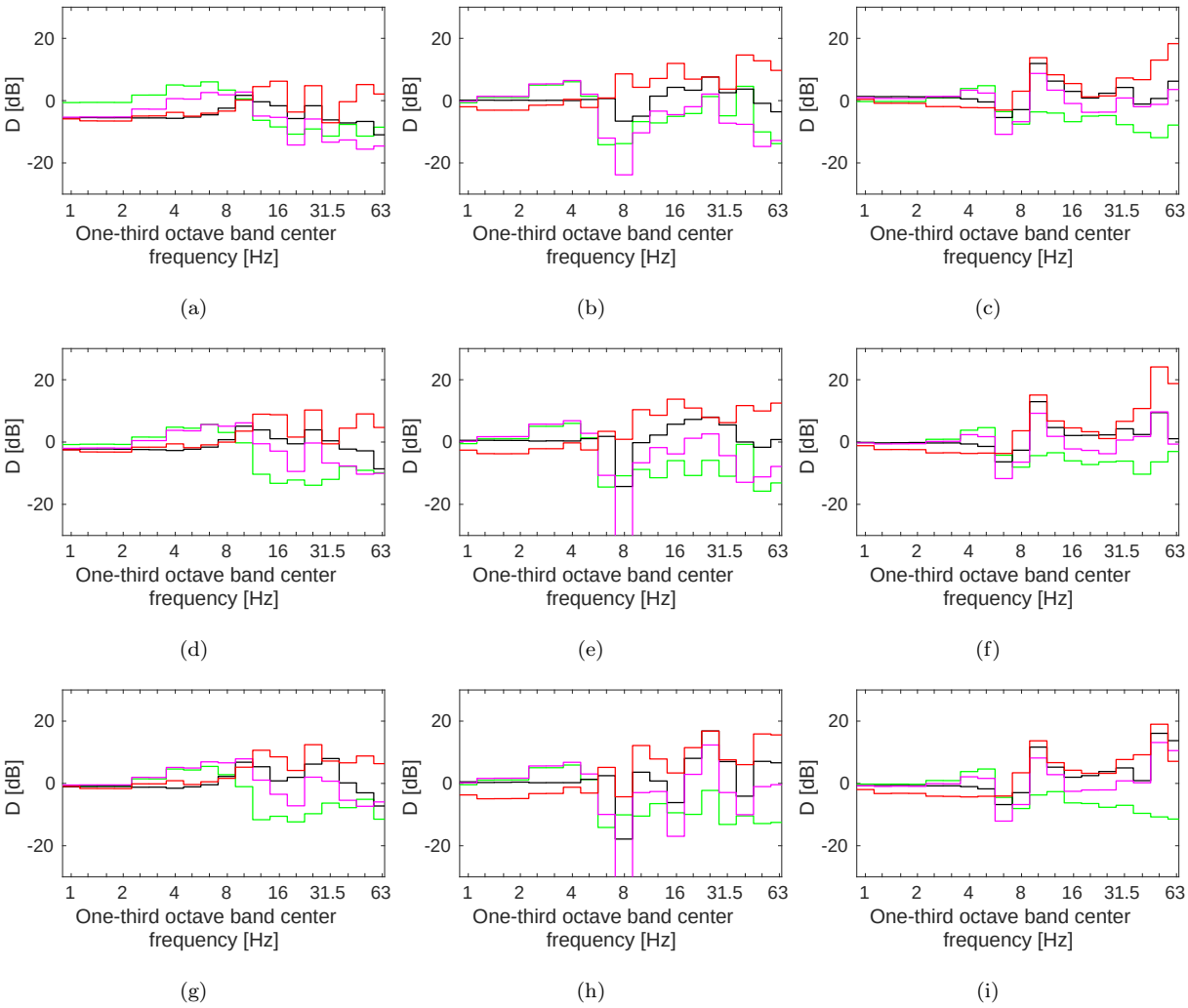

Figure 13: One-third octave band center frequency of the differences at the observation point A of the (a,d,g) four-storey, (b,e,h) six-storey and (c,f,i) twelve-storey buildings, at the (a,b,c) first, (d,e,f) middle and (g,h,i) top floors, from the (green line) simplified methodology D^s, the (black line) approximation I D^I, the (magenta line) approximation II D^{II} and the (red line) solution ignoring SSI $\tilde{D}$.

In order to assess the accuracy of the proposed solutions described in Section 2.2, Figures 13 and 14

show the differences with respect to the reference model. These differences are evaluated as:

$$D^s = 20\log 10\,(u^s/u^r)$$
$$\tilde{D}^s = 20\log 10\,(\tilde{u}/u^r)$$
$$D^I = 20\log 10\,\left(u^I/u^r\right)$$
$$D^{II} = 20\log 10\,\left(u^{II}/u^r\right)$$

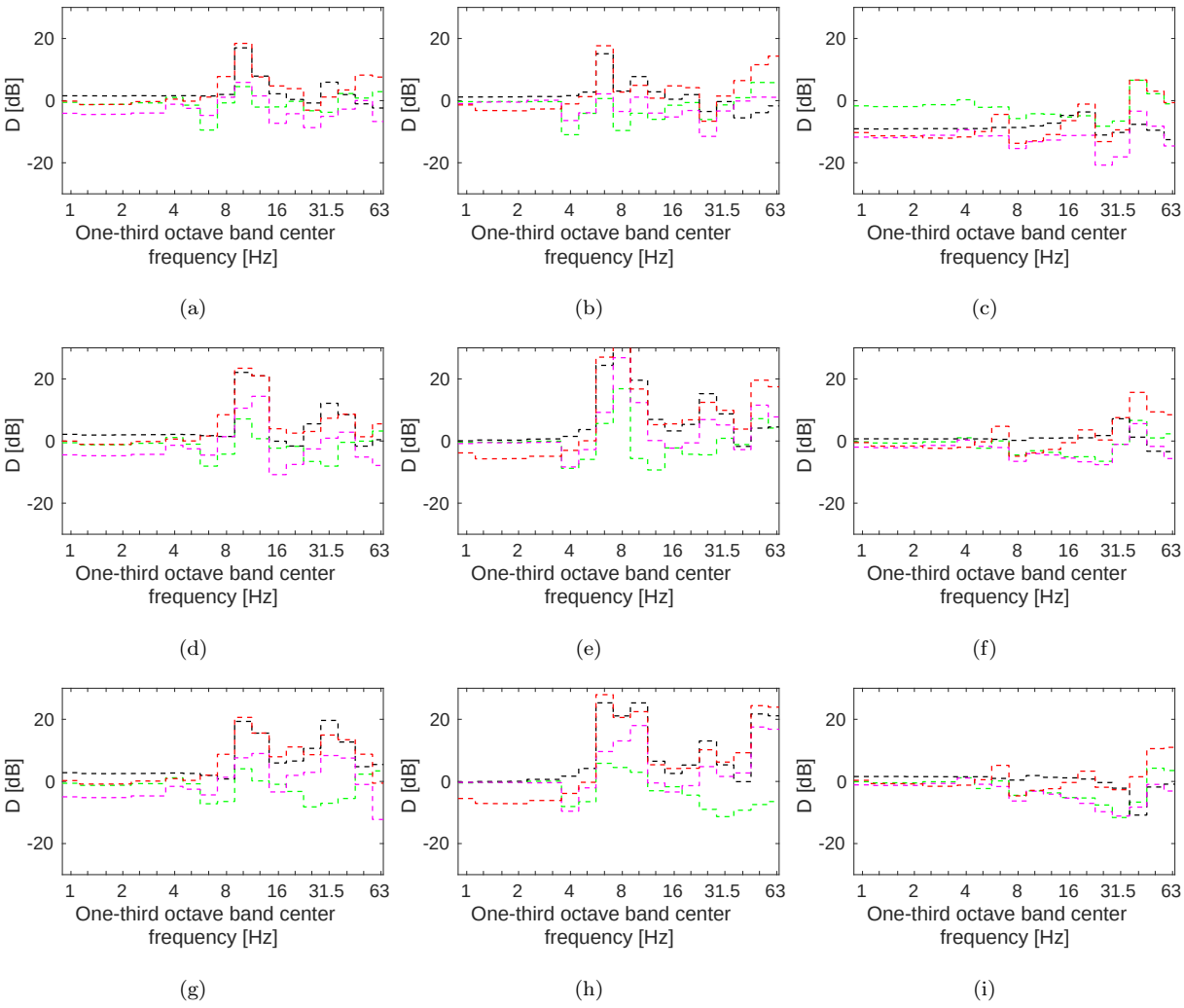

Figure 14: One-third octave band center frequency of the differences at the observation point B of the (a,d,g) four-storey, (b,e,h) six-storey and (c,f,i) twelve-storey buildings, at the (a,b,c) first, (d,e,f) middle and (g,h,i) top floors, from the (green line) simplified methodology D^s, the (black line) approximation I D^I, the (magenta line) approximation II D^{II} and the (red line) solution ignoring SSI $\tilde{D}$.

It is seen that the agreement of the simplified method is reasonably good and this presents the better aproximation with discrepancies up to 16 dB. As expected, the response ignoring SSI overestimates the

result. These amplifications are partly modulated with the coupling loss C_l^r computed from the reference model as shown by the curve D^I. Also, the proposed solutions u^s, u^I and u^{II} are in the same range of uncertainty.

The discrepancies between the reference model maximum transient vibration value (MTVV) [21] response u^r and the solutions u^s, $\tilde{u}$, u^I and u^{II} are shown in Figure 15, depending on storey level. The amplification of the solution ignoring SSI is not greatly modulated by the coupling loss C_l^r proposed in the solution u^I. In spite of the discrepancies, the solutions u^r, u^I and u^{II} give acceptable predictions. The accuracy is similar to the uncertainty range (5 dB to 20 dB) as found in previous research [56–58]. The simplified method presents improved better results compared to the alternative solutions, so therefore is used for analysis in the next section.

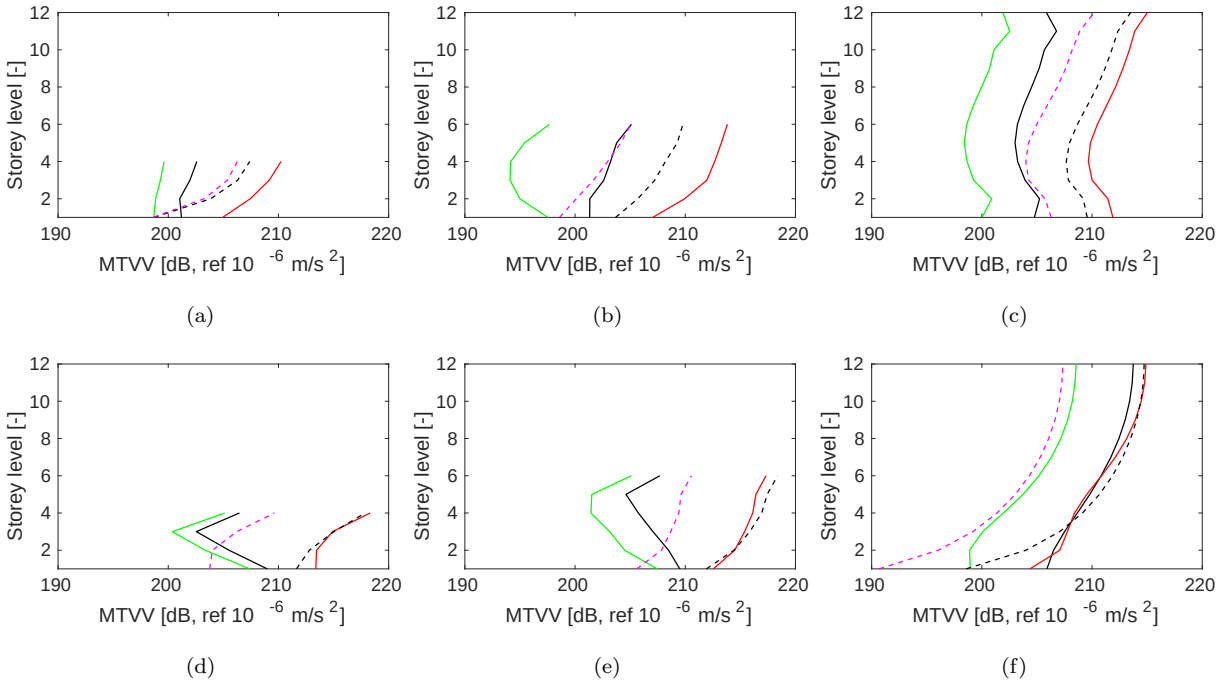

Figure 15: MTVV due to an incident wave field evaluated at the observation points (a,b,c) A and (d,e,f) B of the (a,d) four-storey, (b,e) six-storey and (c,f) twelve-storey buildings computed from the (solid black line) `SSIFiBo` toolbox and the (green line) simplified method. Superimposed are the responses of the (dashed black line) approximation I, the (dashed magenta line) approximation II and (red line) ignoring SSI.

4. Case study: railway track defects

Within the railway vibration cases possible to study, the proposed methodology is now used to analyse building vibration due to local track defects. The building response is calculated by combining the free-field u_g response due to railway traffic with the soil-structure transfer function $u(f)/u_g(f) = F_a(f)C_l(f)$ (Equa-

tion (4)) due to an incident wave field. Free-field response is calculated using a methodology validated in Reference [47]. This facilitates reduced running times because the soil-structure transfer function $u(f)/u_g(f)$ does not depend on the train passage and is only evaluated once for each soil. It should be noted that a comparison between the proposed methodology and the reference model is not included because remembering the free-field vibration u_g is the same for both models, the discrepancies

$$D^s = 20\log 10\left((F_a^s(f)C_l^s(f)u_g(f))/(F_a^r(f)C_l^r(f)u_g(f))\right) = 20\log 10\left((F_a^s(f)C_l^s(f))/(F_a^r(f)C_l^r(f))\right)$$

are identical to those obtained previously (Figures 13 and 14). Therefore, the simplified method allows performing the next analysis with an acceptable accuracy.

A sensitivity analysis of the effect of soil properties, defect type, defect size and train speed is presented. Vibrations are obtained for the buildings analysed previously in Section 3 (Figure 5).

The influence of soil properties on the building response is studied using 3 homogeneous and 2 layered soils. Table 2 contains their properties.

Table 2: Soil properties.

		h [m]	E [MPa]	ν [−]	ξ [−]	ρ [kg/m^3]	V_{s30} [m/s]
Soil 1	Half-space	∞	50	0.35	0.05	2000	96.2
Soil 2	Half-space	∞	100	0.35	0.05	2000	136.1
Soil 3	Half-space	∞	200	0.35	0.05	2000	192.5
Soil 4	Layer 1	2	50	0.35	0.05	2000	180.4
	Half-space	∞	200	0.35	0.05	2000	
Soil 5	Layer 1	2	200	0.35	0.05	2000	99.5
	Half-space	∞	50	0.35	0.05	2000	

Figure 16 shows the singular defects considered in the analysis, where v_0 is the train speed, h the defect height and l the defect length.

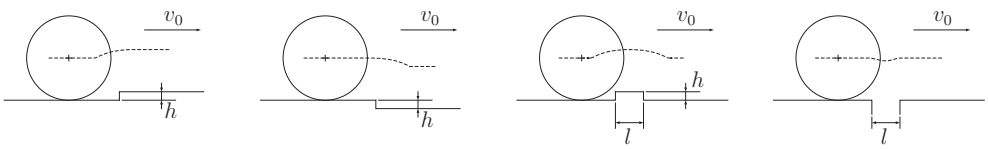

Figure 16: Local defect shape (from left to right: step up, step down, positive pulse, negative pulse).

Moreover the defect size influence on building vibrations is analysed considering several defect lengths $l = \{80, 110, 140, 170, 200\}$ mm.

Regarding the vehicle, a AM96 intercity train (Figure 17) travelling on a ballasted track is considered (Table 4). Moreover the passage of a classic tram (Figure 19) on an urban slab track (Table 5) is studied. The vehicles are modelled using a detailed multibody vehicle approach [59] (Figure 18). AM 96 and classic tram properties are related in Table 3.

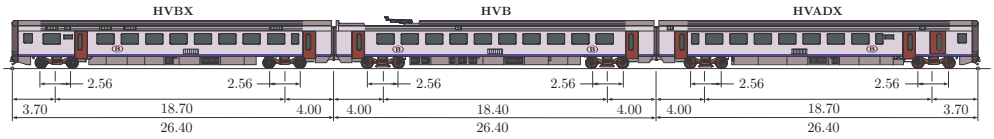

Figure 17: AM96 train dimensions.

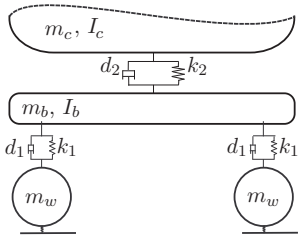

Figure 18: Bogie modelling of AM 96 train and classic tram.

Table 3: AM96 train properties.

		m_c [kg]	I_c [kg m^2]	m_b [kg]	I_b [kg m^2]	m_w [kg]	k_1 [MN/m]	d_1 [kNs/m]	k_2 [MN/m]	d_2 [kNs/m]
AM 96	HVB	25200	1.26×10^6	6900	1.52×10^3	1700	1.3	3.7	0.69	22.6
	HVADX	28900	1.45×10^6	7050	1.58×10^3	1700	1.3	3.7	0.69	22.6
	HVBX	25930	1.3×10^6	11800	2.6×10^3	1700	1.81	1.14	0.69	14
Classic tram		7580	8.75×10^4	3530	6.0×10^2	160	5.876	6	0.96	56.25

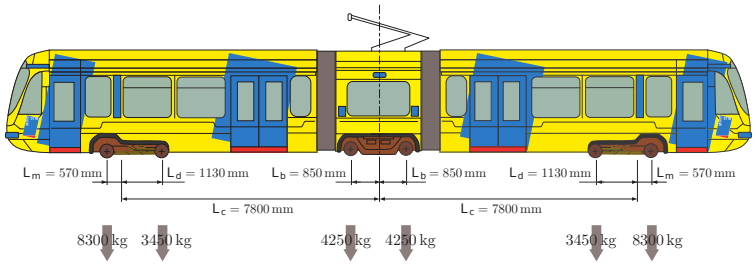

Figure 19: Geometrical configuration of the classic tram.

Table 4: Ballasted track properties.

Ballast track properties (2 rails)	
Track gauge [m]	1.435
Rail 2nd moment of area $\left[\mathrm{m}^4\right]$	3.09×10^{-5}
Rail Young's modulus $\left[\mathrm{N/m}^2\right]$	2.1×10^{11}
Rail density $\left[\mathrm{kg/m}^3\right]$	7850
Railpad stiffness per unit length (2 rails) $\left[\mathrm{N/m}^2\right]$	6.15×10^8
Railpad damping per unit length (2 rails) $\left[\mathrm{Ns/m}^2\right]$	1.2×10^4
Sleeper spacing [m]	0.65
Sleeper mass per unit length [kg/m]	461.5
Ballast stiffness $\left[\mathrm{N/m}^2\right]$	1.3×10^8
Ballast damping $\left[\mathrm{Ns/m}^2\right]$	1.3×10^5
Ballast density $\left[\mathrm{kg/m}^3\right]$	1700
Ballast height (below sleeper) [m]	0.3
Ballast cross-sectional area $\left[\mathrm{m}^2\right]$	0.59
Ballast Poisson's ratio	0.3

Train passages at $v_0 = \{60{,}90{,}120{,}150\}$ km/h and $v_0 = \{20{,}30{,}40{,}50\}$ km/h for the AM96 train and the the classic tram are analysed respectively. The train speeds are below the critical velocity of the track-ground system [60–62].

The midpoint of the building foundation is located at a distance $d = 20$ m from the track centreline and the observation point B (Figure 5) is selected because it presents the highest response (Figure 15). Also, building vibrations are calculated considering a single point response (SPR) excitation model, where the free-field vibration is transmitted simultaneously to the whole building foundation.

4.1. Soil properties

This section analyses the effect of soil properties on building vibrations, considering the passage of the AM96 train at $v_0 = 120$ km/h, over a ballasted track, in the presence of a negative pulse defect.

The free-field response v_g and the simplified method to consider SSI both depend on the soil properties. Figure 20 shows the free-field velocity v_g and the soil-structure transfer function v/v_g in the frequency domain. In the free-field response (Figure 20. (a)), dominant frequencies are located at mid frequencies due to dynamic excitation. These dominant frequencies increase with the soil stiffness varying from 14 to 22 Hz for the softest soil, to 35 and 56 Hz for the stiffest soils. Moreover, the influence of soil stratigraphy in the free

Table 5: Slab track properties.

Slab track properties (2 rails)	
Track gauge [m]	1.435
Rail 2nd moment of area $[\mathrm{m}^4]$	3.09×10^{-5}
Rail Young's modulus $\left[\mathrm{N/m}^2\right]$	2.1×10^{11}
Rail density $\left[\mathrm{kg/m}^3\right]$	7850
Railpad stiffness per unit length (2 rails) $\left[\mathrm{N/m}^2\right]$	4×10^8
Railpad damping per unit length (2 rails) $\left[\mathrm{Ns/m}^2\right]$	1.2×10^4
Slab thickness [m]	0.3
Slab width [m]	2.5
Slab stiffness (concrete) $\left[\mathrm{N/m}^2\right]$	3×10^{10}
Slab 2nd moment of area $[\mathrm{m}^4]$	5.63×10^{-3}
Slab density (concrete) $\left[\mathrm{kg/m}^3\right]$	2500
Slab Poison's ratio (concrete)	0.2

field is shown. In spite of the small thickness of the uppermost layer ($h_1 = 2\,\mathrm{m}$), the dominant frequencies at the medium-high range depends on strongly the properties of this layer. The dominant frequencies of layered soil 4 (Table 2) match with those observed in homogeneous soil 1, because both soils have the same properties in the uppermost layer. A similar effect can be observed between layered soil 5 and homogeneous soil 3. At the low frequency range, the dominant frequencies are controlled by the halfspace properties because of the long wavelengths.

In contrast, soil properties have a high influence on the amplitude of the soil-structure transfer function (Figure 20. (b-d)), but the trend of the response is similar for all the soils. The soil-structure transfer function shows amplifications at low and mid frequencies up to 30 Hz, whereas the response is damped at high frequencies. These amplifications are concentrated at 9 and 17 Hz for the four-storey building (Figure 20. (b)), 6 and 14 Hz for the six-storey building (Figure 20. (c)) and 20 Hz for the twelve-storey building (Figure 20. (d)). These frequencies correspond with the natural frequencies of the buildings (Figure 6). The effect of soil stratigraphy on the building response is not observed due to the assumption of considering an equivalent homogeneous soil to model the SSI.

Building vibration due to a railway defect is obtained by combining the free-field response v_g and the soil-structure transfer function shown previously (Figures 20). Figure 21 shows the frequency content and the running RMS value [21] of the building response. At low frequencies, building vibration decreases with soil stiffness (Figure 21. (a,c,e)). This is as expected because the response depends on long wavelengths.

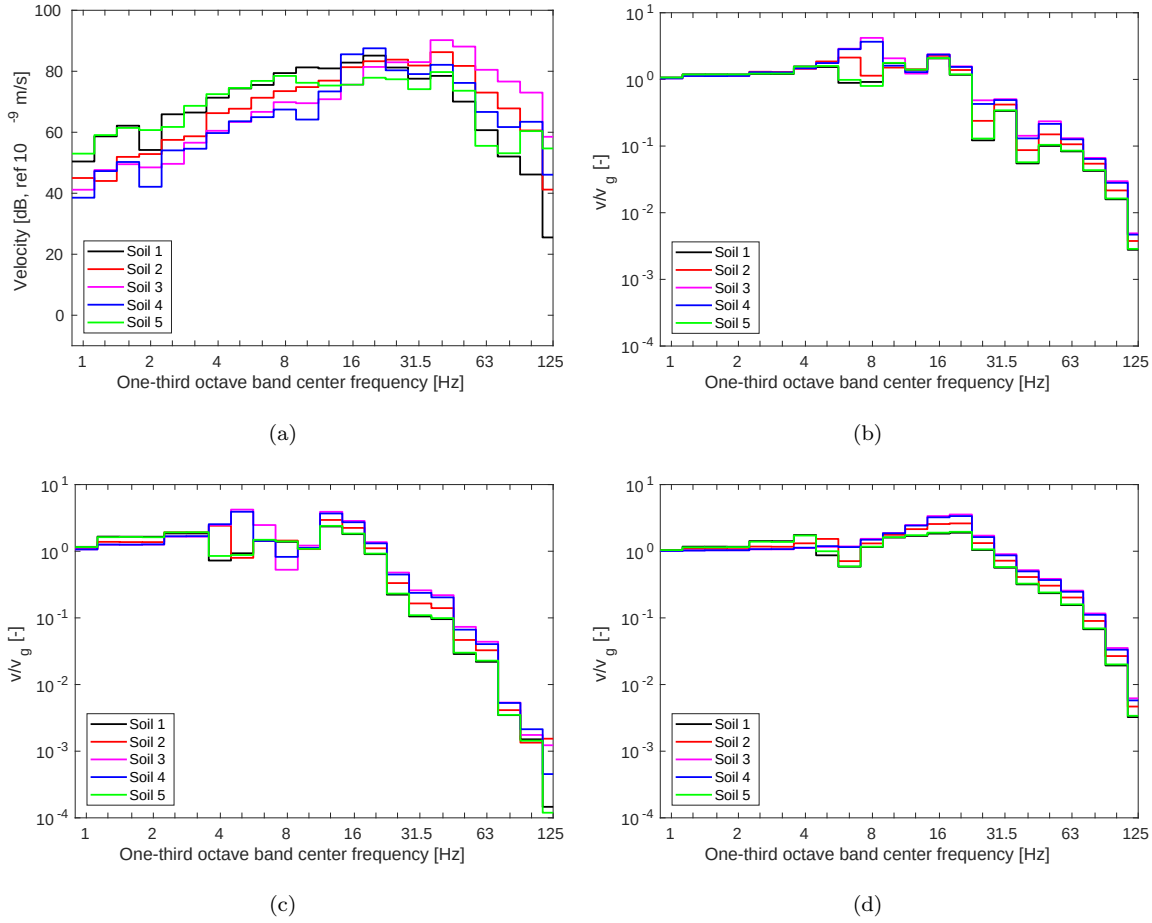

Figure 20: (a) One-third octave band center frequency of the vertical velocity of the free field response v_g at 20 m to the ballasted track due to a AM96 train passage at $v_0 = 120$ km/h and (b-d) soil-structure transfer function v/v_g at the top floor of the (b) four-storey, (c) six-storey and (d) twelve-storey buildings for several soil properties.

In contrast, at high frequencies it is observed an increment of the building response with the soil stiffness. This is consistent with the free-field response v_g (Figure 20. (a)). In addition to the dominant frequencies indicated above, in the soil-structure transfer function v/v_g (Figure 20. (b-d)), the additional frequencies due to the source are significant. Regarding the RMS running value (Figure 21. (b,d,f)), the response of the layered soil with the softest uppermost layer yields the highest vibrations. This is due to the highest free-field response for this soil being approximately 20 Hz (Figure 20. (a)). Although there are higher responses for other soils in the mid-high frequency range, these frequency contents are damped when the responses are weighted to obtain the running RMS values.

4.2. Defect type

This section analyses the influence of defect type on building vibrations for both the AM96 train and the classic tram, on homogeneous soil 2, considering several defect types (Figure 16).

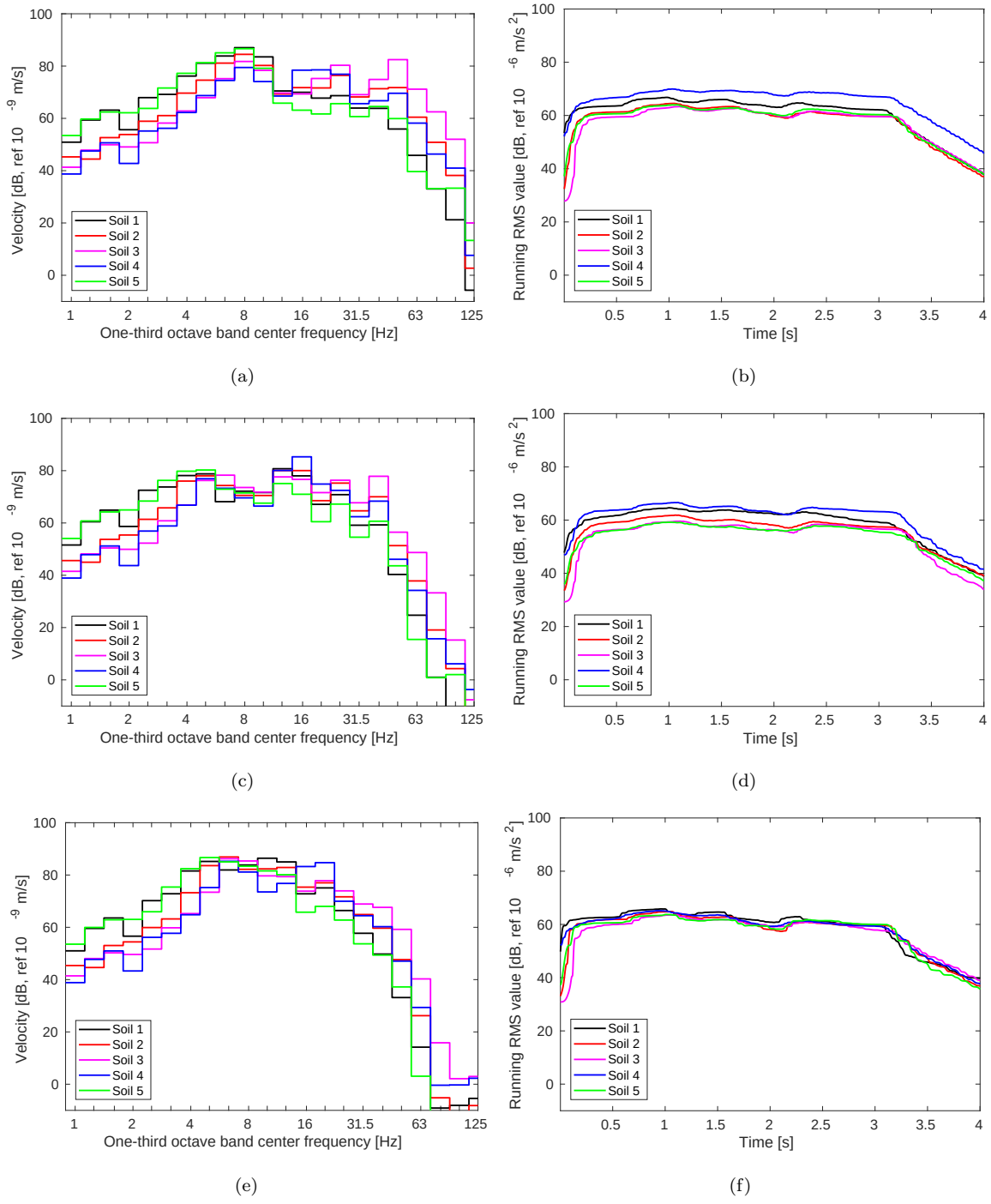

Figure 21: (a,c,e) One-third octave band center frequency of the z vertical velocity and (b,d,f) running RMS value of the weighted acceleration at the top floor of the (a,b) four-storey, (c,d) six-storey and (e,f) twelve-storey buildings for several soil properties due to a AM96 train passage at $v_0 = 120\,\mathrm{km/h}$.

Figure 22 presents the building response due to the AM96 passage over a ballasted track. Overall it can be observed the step up joint induces higher vibrations at low frequencies, whereas the maximum values at mid and high frequencies are due to the positive pulse. Also the defect type influences the amplitude of the response more dominantly than the shape (Figure 22. (a,c,e)). The running RMS values (Figure 22. (b,d,f)) do not show a clear dependency on the defect type because the responses have similar amplitudes.

The building vibrations induced by the classic tram passage over a slab track can be observed in Figure 23. The frequency responses show a similar tendency for all defect types. However, it is more clearly shown in running RMS curves (Figure 23. (b,d,f)) that the highest responses are found for the positive pulse and the step up joint. This is because the response (Figure 23. (a,c,e)) for both defect types yields similar magnitudes in the dominant frequency range from 8 Hz to 20 Hz.

These differences between ballasted (Figure 22) and slab tracks (Figure 23) results show that the type of track is an important parameter to model during vibration assessment.

4.3. Defect size

This section analyses the effect of defect size on building vibrations. Negative pulse defect lengths spanning $l = \{80, 110, 140, 170, 200\}$ mm are considered in the presence of homogeneous soil 2 (Table 2).

Figure 24 shows the building response due to the classic tram passing over a slab track. The correlation between the response amplitude and the defect size is clearly observed in both frequency and time domain curves. The level of vibration increases significantly with the defect size from $l = 80$ to $l = 140$ mm, whereas the building response increases slightly for higher values of defect size.

4.4. Train speed

This section computes several speeds of the AM96 train and the classic tram over the ballasted and slab tracks. The soil is type 2 (Table 2) and the defect is a negative pulse defect. The train speed influence on building vibrations is analysed.

Figure 25 presents building vibrations induced by the AM96 train passage at speeds $v_0 = \{60, 90, 120, 150\}$ km/h. In the frequency domain response (Figure 25. (a,c,e)), the effect of train speed is more clearly shown at low frequencies up to 10 Hz, where the building vibrations increase with the train speed. This trend is not found at mid and high frequencies. The running RMS value curves (Figure 25. (b,d,f)) show again that the level of vibration increases with train speed.

The previous correlation is not evident in the building response due to the classic tram analysis where the speed range is lower (20 versus 50 km/h) (Figure 26). The response is concentrated at frequencies (Figure 26. (a,c,e)) that approximately match with the natural frequencies of the buildings (Figure 6), but the level of vibration at these frequencies has a low correlation with train speed. Thus, the tram speed has a low influence on the running RMS values (Figure 26. (b,d,f)).

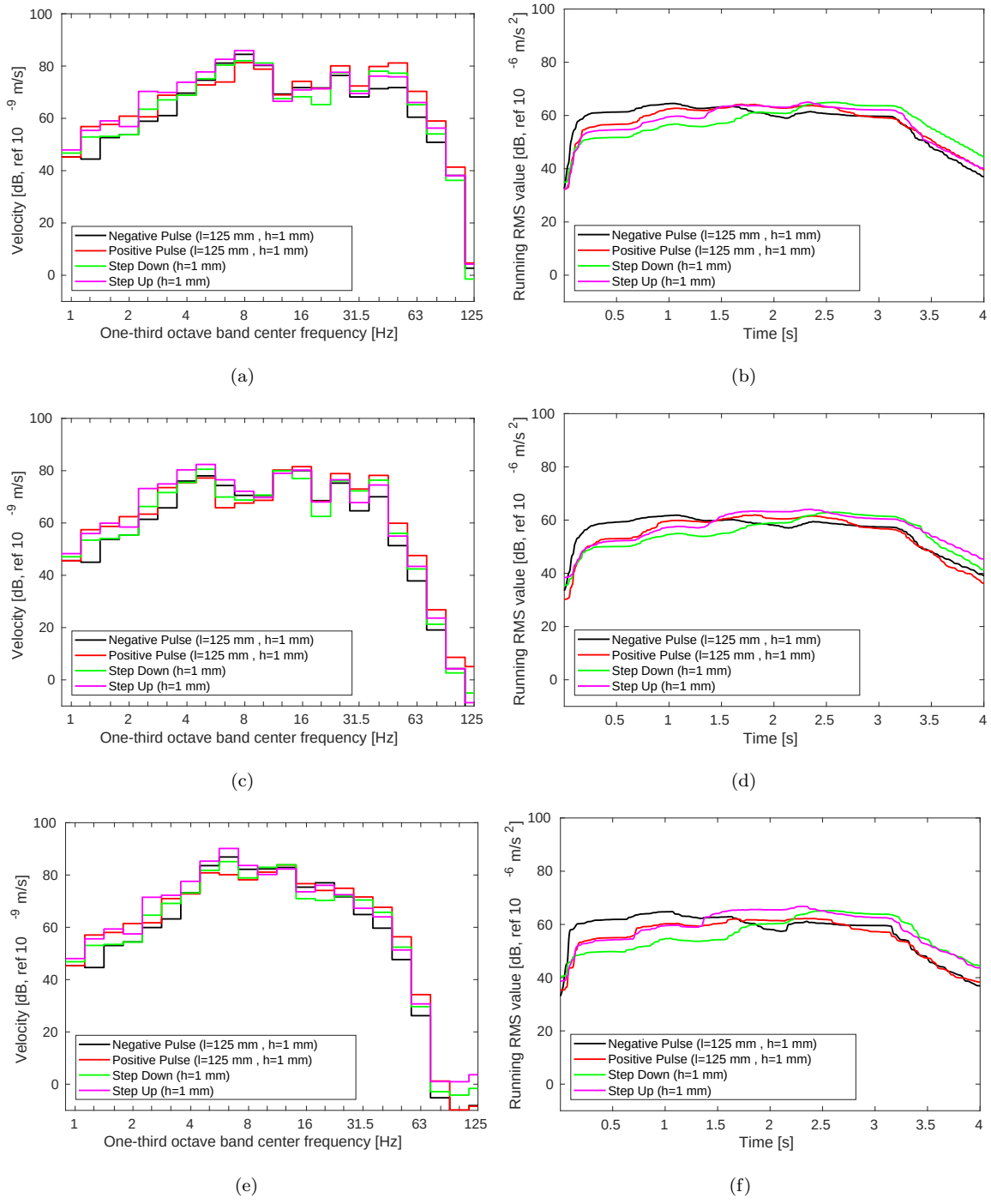

Figure 22: (a,c,e) One-third octave band center frequency of the z vertical velocity and (b,d,f) running RMS value of the weighted acceleration at the top floor of the (a,b) four-storey, (c,d) six-storey and (e,f) twelve-storey buildings for several defect types due to a AM96 train passage at $v_0 = 120\,\mathrm{km/h}$.

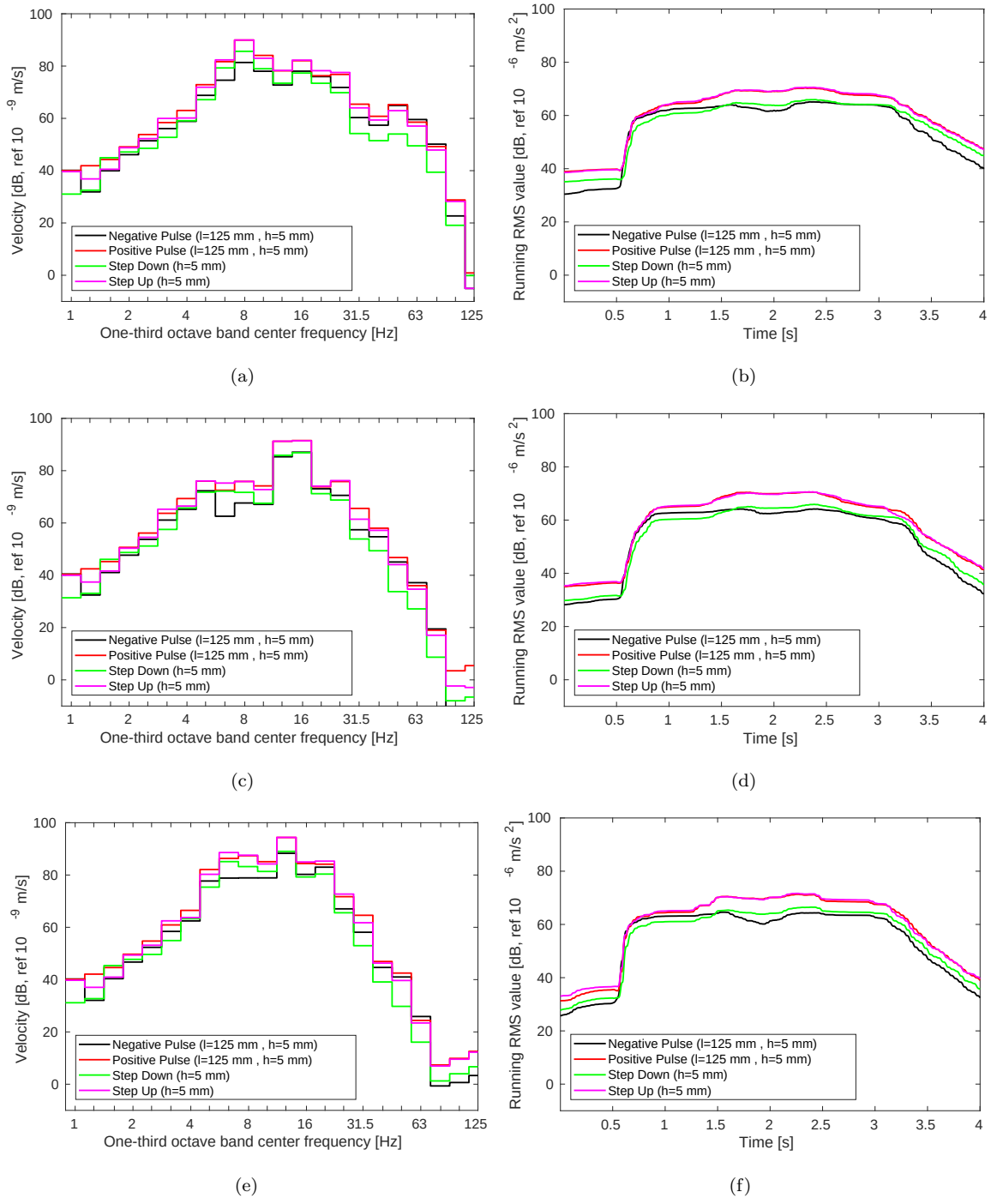

Figure 23: (a,c,e) One-third octave band center frequency of the z vertical velocity and (b,d,f) running RMS value of the weighted acceleration at the top floor of the (a,b) four-storey, (c,d) six-storey and (e,f) twelve-storey buildings for several defect types due to a tram passage at $v_0 = 40\,\mathrm{km/h}$.

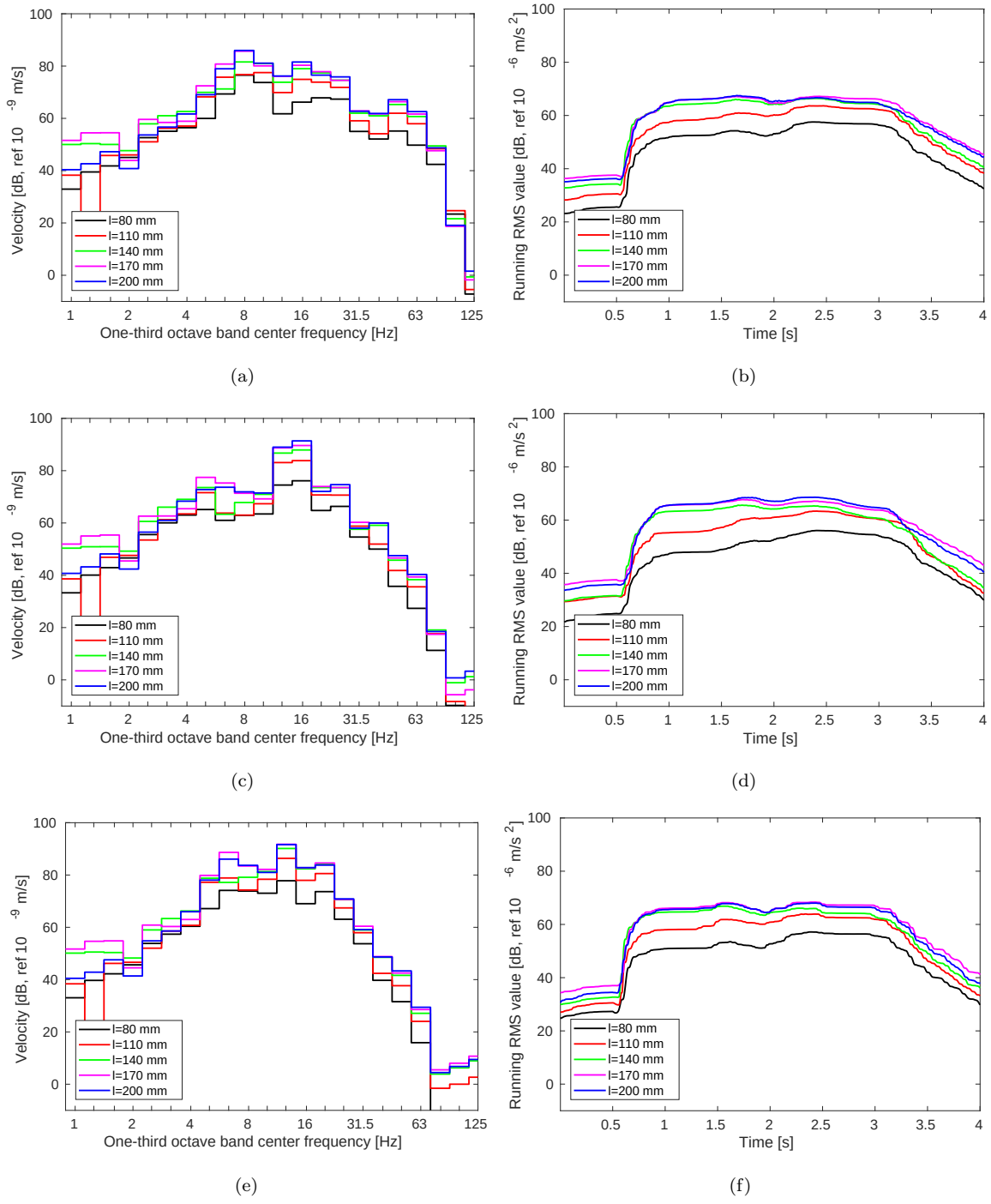

Figure 24: (a,c,e) One-third octave band center frequency of the z vertical velocity and (b,d,f) running RMS value of the weighted acceleration at the top floor of the (a,b) four-storey, (c,d) six-storey and (e,f) twelve-storey buildings for several negative pulse defect sizes due to a tram passage at $v_0 = 40\,\mathrm{km/h}$.

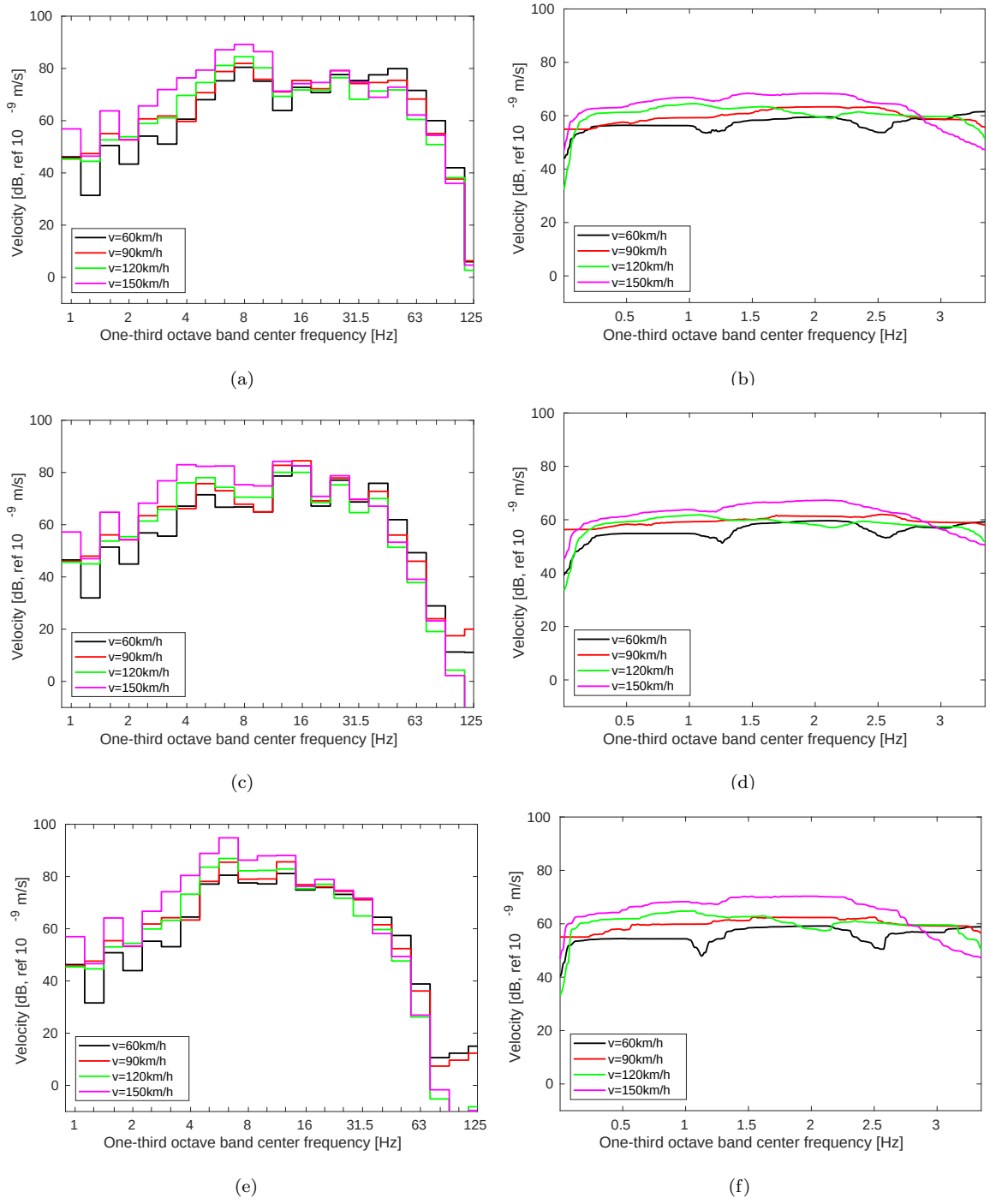

Figure 25: (a,c,e) One-third octave band center frequency of the z vertical velocity and (b,d,f) running RMS value of the weighted acceleration at the top floor of the (a,b) four-storey, (c,d) six-storey and (e,f) twelve-storey buildings due to a AM96 train passage at several speeds and a negative pulse defect.

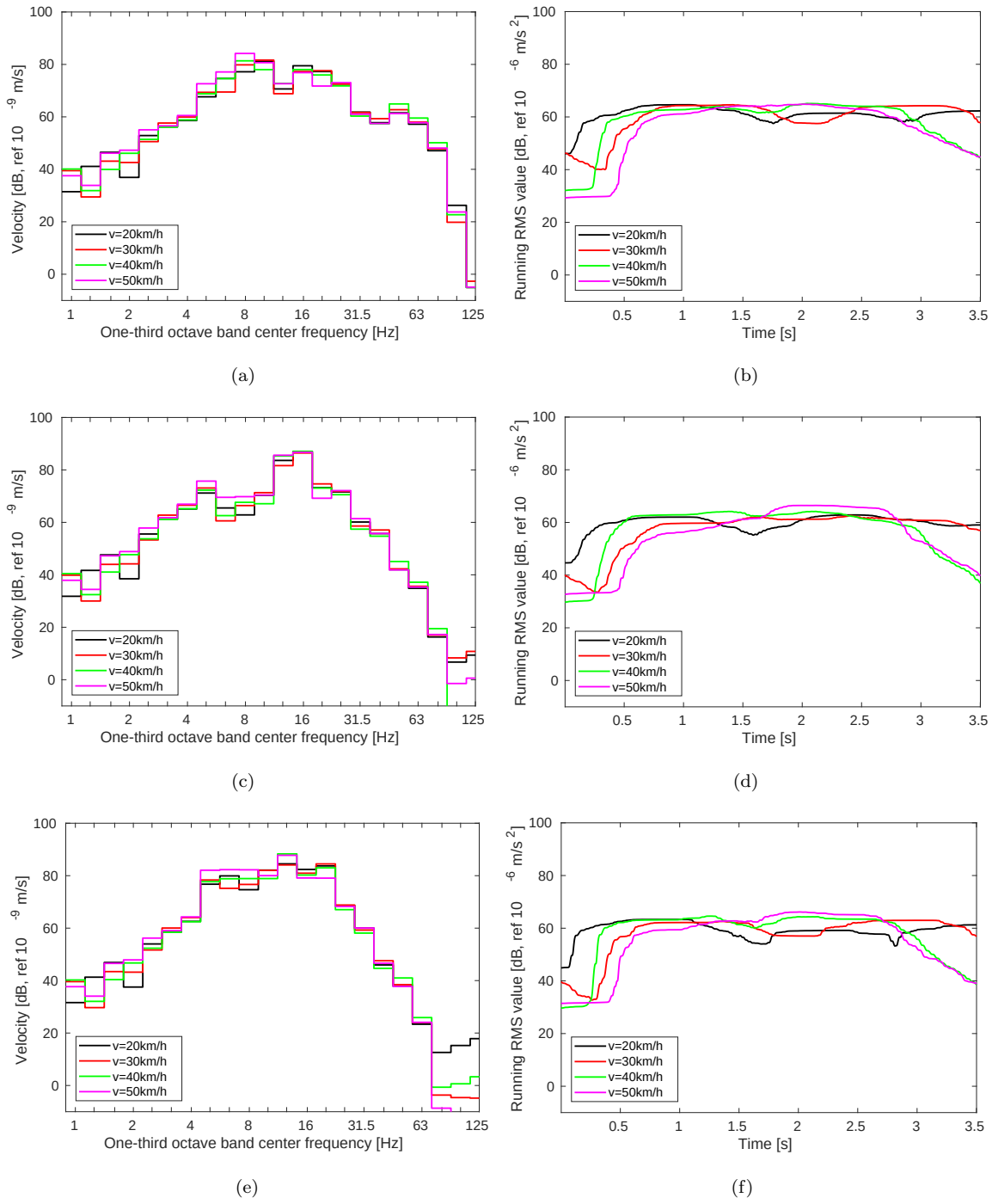

Figure 26: (a,c,e) One-third octave band center frequency of the z vertical velocity and (b,d,f) running RMS value of the weighted acceleration at the top floor of the (a,b) four-storey, (c,d) six-storey and (e,f) twelve-storey buildings due to a tram passage at several speeds and a negative pulse defect.

5. Conclusions

Building vibrations induced by railway traffic is a problem that needs to be studied, during project planning/development phases. To do so, simple methods are useful to assess building vibration quickly, considering multiple scenarios. In this work, a simplified method is presented to do this. It consists of a decoupled model, where the free-field vibration (source and propagation path) and the building vibration (receiver) are computed independently. This proposed paper is focused on the receiver sub-model. The soil-structure transfer function depending on the structural characteristics, and soil properties is obtained. This soil-structure transfer function is combined with the free-field response to obtain the building induced vibration in a computationally efficient manner. The proposed method is verified numerically by comparing results with a comprehensive model.

The dynamic building response due to railway defects is studied. It is found that soil properties, defect type, defect size and train speed have a strong influence on building vibrations.

Acknowledgements

The authors would like to acknowledge the financial support provided by the Spanish Ministry of Economy and Competitiveness (Ministerio de Economía y Competitividad) through research project BIA2016-75042-C2-1-R, the Andalusian Scientific Computing Centre (CICA), the University of Leeds Cheney Award Scheme and the Leverhulme Trust (UK). They also acknowledge the support of Seville, Mons and Leeds Universities, who, without their support, this research would not have been possible.

References

[1] E. Kausel, Early history of soil-structute interaction, Soil Dynamics and Earthquake Engineering 30 (2010) 822–8328. doi:https://doi.org/10.1016/j.soildyn.2009.11.001.

[2] J. Wolf, Dynamic soil-structure interaction, Prentice-Hall, Englewood Cliffs, New Jersey, 1985.

[3] C. Wu, H. Hao, Numerical study of characteristics of underground blast induced surface ground motion and their effect on above-ground structures. part i. ground motion characteristics, Soil Dynamics and Earthquake Engineering 25 (2005) 27 – 38. doi:doi:10.1016/j.soildyn.2004.08.001.

[4] H. Hao, C. Wu, Numerical study of characteristics of underground blast induced surface ground motion and their effect on above-ground structures. part ii. effects on structural responses, Soil Dynamics and Earthquake Engineering 25 (2005) 39 – 53. doi:doi:10.1016/j.soildyn.2004.08.002.

[5] A. Bayraktar, A. Can Altunis, M. Özcan, Safety assessment of structures for near-field blast-induced ground excitations using operational modal analysis, Soil Dynamics and Earthquake Engineering 39 (2012) 23 – 36. doi:dx.doi.org/10.1016/j.soildyn.2012.02.005.

[6] O. Dogan, O. Anil, S.O. Akbas, E. Kantar, R.T. Erdem, Evaluation of blast-induced ground vibration effects in a new residential zone, Soil Dynamics and Earthquake Engineering 50 (2013) 168 – 181. doi:http://dx.doi.org/10.1016/j.soildyn.2013.03.005.

[7] E. Savin, D. Clouteau, Elastic wave propagation in a 3-D unbounded random heterogeneous medium coupled with a bounded medium. application to seismic soil–structure interaction (sssi), International Journal for Numerical Methods in Engineering 54 (2002) 607 – 630. doi:https://doi.org/10.1002/nme.442.

[8] F. Gatti, S. Touhami, F. Lopez-Caballero, R. Paolucci, D. Clouteau, V. A. Fernandes, M. Kham, F. Voldoire, Broad-band 3-D earthquake simulation at nuclear site by an all-embracing source-to-structure approach, Soil Dynamics and Earthquake Engineering 115 (2018) 263 – 280. doi:https://doi.org/10.1016/j.soildyn.2018.08.028.

[9] R. Taherzadeh, D. Clouteau, R. Cottereau, Simple formulas for the dynamic stiffness of pile groups, Earthquake Engineering and Structural Dynamics 38 (2009) 1665 – 1685. doi:https://doi.org/10.1002/eqe.918.

[10] D. Pitilakis, D. Clouteau, Equivalent linear substructure approximation of soil–foundation–structure interaction: model presentation and validation, Bulletin of Earthquake Engineering 8 (2) (2010) 257 – 282. doi:https://doi.org/10.1007/s10518-009-9128-3.

[11] H. Torabi, M. Rayhani, Three dimensional finite element modeling of seismic soil–structure interaction in soft soil, Computers and Geotechnics 60 (2014) 9 – 19. doi:http://dx.doi.org/10.1016/j.compgeo.2014.03.014.

[12] L. Pyl, G. Degrande, G. Lombaert, W. Haegeman, Validation of a source–receiver model for road traffic- induced vibrations in buildings. i: Source model, Journal of Engineering Mechanics 130 (2004) 1377 – 1393. doi:https://doi.org/10.1061/(ASCE)0733-9399(2004)130:12(1377).

[13] L. Pyl, G. Degrande, D. Clouteau, Validation of a source–receiver model for road traffic- induced vibrations in buildings. ii: Receiver model, Journal of Engineering Mechanics 130 (2004) 1394 – 1406. doi:https://doi.org/10.1061/(ASCE)0733-9399(2004)130:12(1394).

[14] S. François, L. Pyl, H. Masoumi, G. Degrande, The influence of dynamic soil-structure interaction on traffic induced vibrations in buildings, Soil Dynamics and Earthquake Engineering 27 (2007) 655–674. doi:https://doi.org/10.1016/j.soildyn.2006.11.008.

[15] D. Connolly, G. Marecki, G. Kouroussis, I. Thalassinakis, P. Woodward, The growth of railway ground vibration problems – A review, Science of the Total Environment 568 (2015) 1276–1282. doi:http://dx.doi.org/10.1016/j.scitotenv.2015.09.101.

[16] G. Kouroussis, S. Zhu, B. Olivier, D. A. W. Zhai, Urban railway ground vibrations induced by localized defects: using dynamic vibration absorbers as a mitigation solution, Journal of Zhejiang University-SCIENCE A 20 (2) (2019) 83 – 97. doi:https://doi.org/10.1631/jzus.A1800651.

[17] S. Zhu, J. Wang, C. Cai, K. Wang, W. Zhai, J. Yang, H. Yan, Development of a vibration attenuation track at low frequencies for urban rail transit, Computer-Aided Civil and Infrastructure Engineering 32 (2017) 713 – 726. doi:https://doi.org/10.1111/mice.12285.

[18] K. Vogiatzis, H. Mouzakis, Ground-borne noise and vibration transmitted from subway networks to multi-storey reinforced concrete buildings, Transport 33 (2) (2018) 446 – 453. doi:https://doi:10.3846/16484142.2017.1347895.

[19] K. Vogiatzis, H. Mouzakis, V. Zafiropoulou, Assessing subway network ground borne noise and vibration using transfer function from tunnel wall to soil surface measured by muck train operation, Science of the Total Environment 650 (2019) 2888 – 2896. doi:https://doi:10.3846/16484142.2017.1347895.

[20] G. Kouroussis, J. Florentin, O. Verlinden, Ground vibrations induced by intercity/interregion trains: a numerical prediction based on the multibody/finite element modeling approach, Journal of Vibration and Control 22 (2016) 4192 – 4210. doi:https://doi.org/10.1177/1077546315573914.

[21] International Organization for Standardization, ISO 2631-1:2003: Mechanical vibration and shock–Evaluation of human exposure to whole-body vibration–Part 1: General requirements (2003).

[22] International Organization for Standardization, ISO 2631-2:2003: Mechanical vibration and shock–Evaluation of human exposure to whole-body vibration–Part 2: Vibration in buildings (1–80 Hz) (2003).

[23] International Organization for Standardization, ISO 14837-1:2005 Mechanical vibration–Ground-borne noise and vibration

arising from rail systems–Part 1: General guidance (2005).

[24] P. Fiala, G. Degrande, F. Augusztinovicz, Numerical modelling of ground-borne noise and vibration in buildings due to surface rail traffic, Journal of Sound and Vibration 301 (2007) 718–738. doi:https://doi.org/10.1016/j.jsv.2006.10.019.

[25] P. Galvín, A. Romero, J. Domínguez, Fully three-dimensional analysis of high-speed train–track–soil–structure dynamic interaction, Journal of Sound and Vibration 329 (2010) 5147–5163. doi:https://doi.org/10.1016/j.jsv.2010.06.016.

[26] D. Cantero, T. Arvidsson, E. OBrien, R. Karoumi, Train–track–bridge modelling and review of parameters, Structure and Infrastructure Engineering 12 (9) (2016) 1051 – 1064. doi:http://dx.doi.org/10.1080/15732479.2015.1076854.

[27] A. Doménech, M. Martínez-Rodrigo, A. Romero, P. Galvín, On the basic phenomenon of soil-structure interaction on the free vibration response of beams: Application to railway bridges, Engineering Structures 125 (2016) 254 – 265. doi:http://dx.doi.org/10.1016/j.engstruct.2016.06.052.

[28] P. Coulier, G. Lombaert, G. Degrande, The influence of source-receiver interaction on the numerical prediction of railway induced vibrations, Journal of Sound and Vibration 333 (2014) 2520–2538. doi:https://doi.org/10.1016/j.jsv.2014.01.017.

[29] C.E. Hanson, D.A. Towers, L.D. Meister, High-speed ground Transportation Noise and Vibration Impact Assessment, HMMH Report 293630-4, U.S. Department of Transportation, Federal Railroad Administration, Office of Railroad Development.

[30] C.E. Hanson, D.A. Towers, L.D. Meister, Transit Noise and Vibration Impact Assessment, Report FTA-VA-90-1003-06, U.S. Department of Transportation, Federal Transit Administration, Office of Planning and Environment.

[31] Federal Railroad Administration, High-Speed Ground Transportation Noise and Vibration Impact Assessment, U.S. Department of Transportation (2012).

[32] W. Rücker, L. Auersch, A user-friendly prediction tool for railway induced ground vibrations: Emission - transmission - immission, Notes on Numerical Fluid Mechanics and Multidisciplinary Design 99 (2008) 129–135. doi:https://dx.doi.org/10.1007/978-3-540-74893-9_18.

[33] L. Auersch, Dynamic stiffness of foundations on inhomogeneous soils for a realistic prediction of vertical building resonance, Journal of Geotechnical and Geoenvironmental Engineering 134 (3) (2008) 328–340. doi:http://dx.doi.org/10.1061/(ASCE)1090-0241(2008)134:3(328).

[34] L. Auersch, Building Response due to Ground Vibration–Simple Prediction Model Based on Experience with Detailed Models and Measurements, International Journal of Acoustics and Vibration 15 (3) (2010) 101–112. doi:http://dx.doi.org/10.20855/ijav.2010.15.3262.

[35] L. Auersch, Wave propagation in the elastic half-space due to an interior load and its application to ground vibration problems and buildings on pile foundations, Soil Dynamics and Earthquake Engineering 30 (2010) 925–936. doi:https://doi.org/10.1016/j.soildyn.2010.04.003.

[36] M. Hussein, H. Hunt, K. Kuo, P. Alves Costa, J. Barbosa, The use of sub-modelling technique to calculate vibration in buildings from underground railways, Proceedings of the Institution of Mechanical Engineers, Part F: Journal of Rail and Rapid Transit 229 (3) (2013) 303 – 314. doi:https://doi.org/10.1177/0954409713511449.

[37] M. Hussein, H. Hunt, K. Kuo, P. Alves Costa, J. Barbosa, The dynamic effect of piled-foundation building on an incicident vibration field from an underground railway tunnel, 20th International Congress on Sound & Vibration. ICSV 20.

[38] G. Kouroussis, L. V. Parys, C. Conti, O. Verlinden, Prediction of ground vibrations induced by urban railway traffic: An analysis of the coupling assumptions between vehicle, track, soil, and buildings, The International Journal of Acoustics and Vibration 18 (4) (2013) 163 – 172. doi:https://doi.org/10.20855/ijav.2013.18.4330.

[39] G. Kouroussis, K.E. Vogiatzis, D.P. Connolly, A combined numerical/experimental prediction method for urban railway vibration, Soil Dynamics and Earthquake Engineering 97 (2017) 377 – 386. doi:http://dx.doi.org/10.1016/j.soildyn.2017.03.030.

[40] G. Kouroussis, K.E. Vogiatzis, D.P. Connolly, Assessment of railway ground vibration in urban area using in-situ trans-

fer mobilities and simulated vehicle-track interaction, International Journal of Rail Transportation 6 (2018) 113 – 130. doi:https://doi.org/10.1080/23248378.2017.1399093.

[41] P. Lopes, P. Alves Costa, M. Ferraz, R. Calçada, A. Silva Cardoso, Numerical modeling of vibrations induced by railway traffic in tunnels: From the source to the nearby buildings, Soil Dynamics and Earthquake Engineering 61–62 (2014) 269–285. doi:https://doi.org/10.1016/j.soildyn.2014.02.013.

[42] P. Lopes, J. Fernández Ruiz, P. Alves Costa, L. Medina Rodríguez, A. Silva Cardoso, Vibrations inside buildings due to subway railway traffic. experimental validation of a comprehensive prediction model, Science of the Total Environment 568 (2016) 1333–1343. doi:http://dx.doi.org/10.1016/j.scitotenv.2015.11.016.

[43] D.P. Connolly, G. Kouroussis, A. Giannopoulos, O. Verlinden, P.K. Woodward, M.C. Forde, Assesment of railway vibrations using an efficient scoping model, Soil Dynamics and Earthquake Engineering 58 (2014) 37–47. doi:https://doi.org/10.1016/j.soildyn.2013.12.003.

[44] D.P. Connolly, G. Kouroussis, P.K. Woodward, A. Giannopoulos, O. Verlinden, M.C. Forde, Scoping prediction of re-radiated ground-borne noise and vibration near high speed rails lines with variable soils, Soil Dynamics and Earthquake Engineering 66 (2014) 78–88. doi:https://doi.org/10.1016/j.soildyn.2014.06.021.

[45] D. López-Mendoza, A. Romero, D. Connolly, P. Galvín, Scoping assessment of building vibration induced by railway traffic, Soil Dynamics and Earthquake Engineering 93 (2017) 147–161. doi:http://dx.doi.org/10.1016/j.soildyn.2016.12.008.

[46] K. Kuo, M. Papadopoulos, G. Lombaert, G. Degrande, The coupling loss of a building subject to railway induced vibrations: Numerical modelling and experimental measurements, Journal of Sound and Vibration 442 (2019) 459–481. doi:https://doi.org/10.1016/j.jsv.2018.10.048.

[47] D.P. Connolly, P. Galvín, B. Olivier, A. Romero, G. Kouroussis, A 2.5D time-frequency domain model for railway induced soil-building vibration due to railway defects, Soil Dynamics and Earthquake Engineering 120 (2019) 332 – 344. doi:https://doi.org/10.1016/j.soildyn.2019.01.030.

[48] O. Zienkiewicz, The finite element method, 3rd Edition, McGraw-Hill, 1986.

[49] N. Newmark, A method of computation for structural dynamics, ASCE Journal of the Engineering Mechanics Division 85 (1959) 67–94.

[50] R. Clough, J. Penzien, Dynamic of Structures, McGraw-Hill, New York, 1975.

[51] European Committee for Standardization, Eurocode 8: Design of structures for earthquake resistance–Part 1 : General rules, seismic actions and rules for buildings (1998).

[52] National Institute of Standards and Technology U.S. Department of Commerce, NIST GCR 12-917-21 Soil-Structure Interaction for Building Structures (2012).

[53] A. Pais, E. Kausel, Approximate formulas for dynamic stiffness of rigid foundations, Soil Dynamics and Earthquake Engineering 7 (4) (1988) 213–227. doi:http://dx.doi.org/10.1016/S0267-7261(88)80005-8.

[54] P. Galvín, A. Romero, A MATLAB toolbox for soil-structure interaction analysis with finite and boundary elements, Soil Dynamics and Earthquake Engineering 57 (2014) 10–14. doi:https://doi.org/10.1016/j.soildyn.2013.10.009.

[55] Deutsches Institut für Normung, DIN 45672 Teil 2: Schwingungsmessungen in der Umgebung von Schienenverkehrswegen: Auswerteverfahren (1995).

[56] G. Lombaert, P. Galvín, S. François, G. Degrande, Quantification of uncertainty in the prediction of railway induced ground vibration due to the use of statistical track unevenness data, Journal of Sound and Vibration 333 (18) (2014) 4232 – 4253. doi:https://doi.org/10.1016/j.jsv.2014.04.052.

[57] S. Jones, K. Kuo, M.F.M. Hussein, H.E.M Hunt, Prediction uncertainties and inaccuracies resulting from common assumptions in modelling vibration from underground railways, Proceedings of the Institution of Mechanical Engineers, Part F: Journal of Rail and Rapid Transit 226 (2012) 501–512. doi:https://doi.org/10.1177/0954409712441744.

[58] D.P. Connolly, P. Alves Costa, G. Kouroussis, P. Galvín, P.K. Woodward, O. Laghrouche, Large scale interna-

tional testing of railway ground vibrations across Europe, Soil Dynamics and Earthquake Engineering 71 (2015) 1–12. doi:https://doi.org/10.1016/j.soildyn.2015.01.001.

[59] G. Kouroussis, D.P. Connolly, K.E. Vogiatzis, O. Verlinden, Modelling the environmental effects of railway vibrations from different types of rolling stock: a numerical study, Shock and Vibration 6. doi:http://dx.doi.org/10.1155/2015/142807.

[60] P. Alves Costa, A. Colaço, R. Calçada, A. Silva Cardoso, Critical speed of railway tracks. Detailed and simplified approaches, Transportation Geotechnics 2 (2015) 30–46. doi:https://doi.org/10.1016/j.trgeo.2014.09.003.

[61] S. B. Mezher, D. P. Connolly, P. K. Woodward, O. Laghrouche, J. Pombo, P. A. Costa, Railway critical velocity – analytical prediction and analysis, Transportation Geotechnics 6 (2016) 84 – 96. doi:https://doi.org/10.1016/j.trgeo.2015.09.002.

[62] K. Dong, D. P. Connolly, O. Laghrouche, P.K. Woodward, P. Alves Costa, The stiffening of soft soils on railway lines, Transportation Geotechnics 17 (A) (2018) 178 – 191. doi:https://doi.org/10.1016/j.trgeo.2018.09.004.